Design of a passive overground body weight support system with forward force:

Theory, conception & realization

J. B. J. van der Schaaf

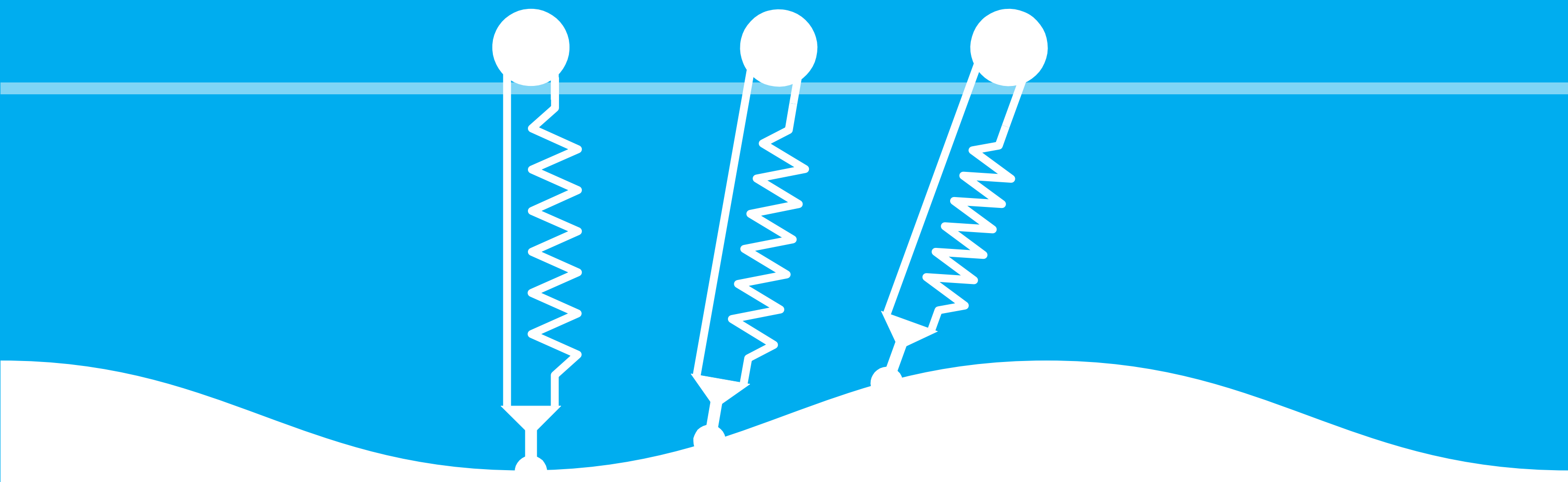

TU Delft

Design of a passive overground body weight support system with forward force: Theory, conception & realization

by

J. B. J. van der Schaaf

to obtain the degree of Master of Science
at the Delft University of Technology,
to be defended publicly on Tuesday 21 August 2018 at 14:00.

Student number:	4088174	
Project duration:	September 1, 2017 – August 21, 2018	
Thesis committee:	Prof. dr. ir. Heike Vallery,	TU Delft, supervisor
	Prof. dr. ir. Martijn Wisse,	TU Delft, external member
	Ir. Andrew Berry,	TU Delft, supervisor

This thesis is confidential and cannot be made public until August 21, 2023.

An electronic version of this thesis is available at `http://repository.tudelft.nl/`.

TU Delft

Abstract

Gait rehabilitation attempts to alleviate gait and balance impairments caused by spinal cord injury. Conventional gait rehabilitation often includes unloading a portion of the user's weight with a vertical force. This vertical force enables people to practice stepping but makes forward propulsion more difficult. Users will adopt a compensatory movement strategy during rehabilitation that may not completely transfer to unsupported walking. It is hypothesized that including a small forward force during vertical unloading makes gait rehabilitation more similar to unsupported locomotion.

This thesis presents and investigates a novel patent of a device that passively generates a forward to propel the user forward. The forward force is generated using the vertical oscillations that naturally occur during gait. This thesis quantifies the forward force, simulates the impact on human gait and details the construction of a prototype. The prototype is then used to validate the simulations of the device.

Analysis indicates that the ratio between the sprocket radius and the wheel radius is the key parameter for determining the amount of forward force. Simulations in which the device is coupled with the spring-loaded inverted pendulum model indicate that the device may generally deteriorate the walking velocity, step size and maximum height difference. Experiments with the prototype indicate that friction has a big effect on the functionality of the device, and that predictions from the simulation may be quantitatively off.

The device may have a favorable interaction with the neurological control strategy of human gait, which was not modeled. Human trials will have to give a definite answer.

Acknowledgements

I would like to thanks my supervisors, Andy Berry, Daniel Lemus and Heike Vallery for their never-ending feedback. Without their feedback, ranging from small screws to long rails and from unnecessary details to overlooked ideas, this thesis would not have been possible.

Additionally, I would also like to thank the people at the workshop, Jan, Reinier, Wim and Dries, for their support in turning (both figuratively and on a lathe) the prototype into reality.

I would like to give special thanks to Aureja, Jesús, Robert and Salil for keeping me company in the basement. I outlasted you all, but now I am escaping as well.

Finally, I would like to thank Sanne, whose ever-lasting patience will finally be rewarded.

Jurriën van der Schaaf

Contents

1 Introduction **1**
- 1.1 Gait Rehabilitation & Body Weight Support . . . 1
- 1.2 Propulsion & Body Weight Unloading . . . 2
  - 1.2.1 Propulsion . . . 2
  - 1.2.2 Effects of Body Weight Support & Forward Forces on Propulsion. . . . 2
- 1.3 Need for Forward Force . . . 3
- 1.4 Patent: a Passive BWS Device for Forward Forces . . . 3
  - 1.4.1 Motivation . . . 3
  - 1.4.2 Working Principle . . . 4
- 1.5 Contributions of this Thesis . . . 5

2 Theoretical Concept Realization **7**
- 2.1 Static Analysis . . . 7
  - 2.1.1 Introduction . . . 7
  - 2.1.2 Methods: Free-body Diagram . . . 7
  - 2.1.3 Results . . . 9
  - 2.1.4 Discussion . . . 9
- 2.2 Dynamic Analysis: Combination with SLIP Model . . . 10
  - 2.2.1 Introduction . . . 10
  - 2.2.2 Methods: Numerical Simulation . . . 10
  - 2.2.3 Results . . . 12
  - 2.2.4 Discussion . . . 13

3 Mechanical Concept Realization **15**
- 3.1 Introduction: Design Requirements. . . . 15
  - 3.1.1 Functional objectives . . . 15
  - 3.1.2 Safety objectives . . . 15
  - 3.1.3 Wish List . . . 15
  - 3.1.4 Safety Factors . . . 16
- 3.2 Methods: Component & Material Selection . . . 16
  - 3.2.1 Wheel & Flange . . . 16
  - 3.2.2 O-ring . . . 17
  - 3.2.3 Chain . . . 17
  - 3.2.4 Sprocket . . . 17
  - 3.2.5 Freewheel . . . 17
  - 3.2.6 Spring . . . 18
- 3.3 Results . . . 18
- 3.4 Discussion . . . 18

4 Evaluation **21**
- 4.1 Introduction . . . 21
- 4.2 Methods: Motion-capture Experiments . . . 21
- 4.3 Results: Response to Input Trajectory . . . 21
- 4.4 Discussion . . . 22

5 Discussion **27**
- 5.1 Evaluation . . . 27
- 5.2 Mechanical Concept Realization . . . 27
- 5.3 Theoretical Concept Realization . . . 27
- 5.4 Introduction . . . 28

6 Conclusion 29
6.1 Summary 29
6.2 Future Work. 29

A Simulation 31
A.1 Equations of Motion 31
A.2 Ratchet Constraint 33
A.3 Slack Chain Constraint 33
A.4 Numerical Integration 34

B Force Plate Data 37

C Technical Drawings 39

Bibliography 55

1

Introduction

1.1. Gait Rehabilitation & Body Weight Support

Gait and balance impairments are a health issue that prevent people from performing many activities of daily living, and often prevent them from living independently. Gait rehabilitation attempts to alleviates the gait and balance impairments through training, restoring independence and enabling people to perform activities of daily living again.

Gait and balance impairments are often caused by diseases like stroke or spinal cord injury (SCI). Stroke and SCI cause neurological defects which may target the spinal circuits that control gait and balance. These neurological defects may lead to reduced muscle activity, reduced weight-bearing capability and reduced balance [1]. If people survive the initial trauma of these conditions, they will often live as long as people without these conditions. Without treatment, the gait and/or balance impairments caused by the stroke or SCI become permanent though, and people suffering from them require lifelong care. This care is costly, which means that treating the gait and balance impairments would greatly reduce the cost of care. In addition, people with gait and balance impairments are also prone to direct additional injury from, for example, falls, as well as indirect injury stemming from the lack of physical exercise such as obesity or bedsores.

Gait rehabilitation aims to improve or restore mobility, helping people regain their independence and ability to contribute to society [2]. Gait rehabilitation, or gait training takes place in a safe environment where the users are protected from falls, as well as being assisted with their movements. Essential to this is the unloading of body weight. Firstly, weight unloading helps users bear their weight, which is generally difficult for people with gait and balance impairments. Secondly, weight unloading helps people with balance (reduced eigenfrequency). Thirdly, unloading weight allows people to practice stepping [3]. Being able to practice stepping is especially important for it allows users to perceive sensory feedback of load-bearing of their feet, which is critical to relearning gait [2–5]. Furthermore, the amount of body weight that is unloaded can be modulated. It can be high at first, and gradually lowered as the user progresses through their training. This enables the therapy to start soon after the initial trauma [3].

Assisting gait rehabilitation is very mechanical by nature, and lends itself well to robotization [6]. Robotization reduces the labor intensity and thereby increases the availability and also increases the consistency by reducing trainer fatigue and trainer inter-variability [2].

These robotic interfaces are often controlled and either apply forces to the legs, or suspend a person from the trunk, allowing the user to freely move their legs. Trunk-supporting systems, used in both treadmill and overground environments, are more popular because the guidance provided by constraining the legs reduces motor learning [6]. Overground rehabilitation proved to be much more task-specific to actual walking than treadmill rehabilitation [5, 7–10]. Task-specificity refers to how well training one exercise helps people become better at a different exercise. For example, ice (speed) skaters may go inline skating in the summer. Inline skating targets the same muscle groups, the same action of the muscle (concentric, eccentric, isometric), the same range of motion of the muscle and the same speed or angular velocity of the muscle action, and can therefore be considered task-specific to ice skating [9]. Treadmill rehabilitation does not train people to generate propulsive forces at the end of stance period, and therefore it is not task-specific to walking [8].

1.2. Propulsion & Body Weight Unloading

1.2.1. Propulsion

Locomotion is the ability to move through the environment, from one place to another. It is the most dictating factor in the morphology and physiology of humans and all other animals [11]. Locomotion is almost always produced by appendages or bodies that oscillate, undulate, pulsate or undergo peristaltic motion. As a result of this, the forces that are exerted on the environment are also oscillating, or otherwise periodic [11]. Despite the periodic propulsive forces, the center of mass of humans (and all other animals) moves at a more or less uniform horizontal rate. By storing kinetic energy as gravitational energy (during walking) or as strain energy (during running) humans are able to keep their forward kinetic energy nearly constant, despite periodic energy exchanges with the environment [11].[1]

By Newton's third law, every force that the human exerts on the environment is coupled with a reactive force exerted on the human. Humans push off against the ground to propel themselves forward. Together, the propulsive forces and the dynamic loading force that the human exerts on the ground due to his or her mass constitute the total ground reaction force (GRF). Generally, in normal walking, the GRF vector points to the hip joint, minimizing torques on the hip joint [11, 12]. This soft direction constraint, caused by the evolutionary desire to walk energy-efficiently, couples the weight-bearing part and the propelling part of the GRF. The reason humans need to constantly propel themselves forward, even when walking at a constant speed on a level ground, is because energy is lost to ground impact, negative work in muscles and to a lesser extent air drag.

In normal human walking gait, literature has identified three power events that deliver energy for forward propulsion [9, 13–15].

- Ankle plantar flexion at push-off
- Hip extension in early stance phase
- Hip flexion in terminal stance and early swing phase

Figure 1.1 shows the power events as they occur during a single gait cycle.

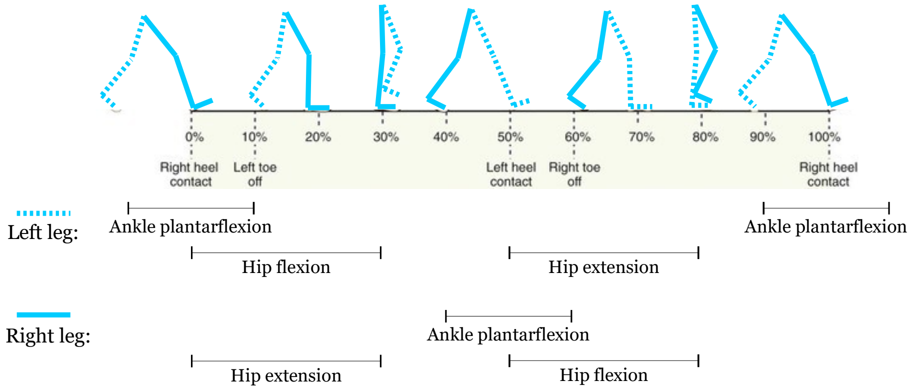

Figure 1.1: Schematic overview of the power events during a single gait cycle. Timing data from [13]

1.2.2. Effects of Body Weight Support & Forward Forces on Propulsion

People with gait and balance impairments are often treated using a body-weight support (BWS) system. Conventional BWS systems provide a vertical upwards force on the user's trunk or pelvis. This vertical force reduces the static weight bearing part of the GRF, but also inevitably reduces the propulsive part of the GRF [8, 11, 16]. Furthermore, the increased vertical unloading force is associated with a decreased walking speed, caused by a decreased step length and unaffected cadence [17, 18]. It has been hypothesized that the weight unloading reduces the GRF, and the reduced GRF may lead to reduced propulsion and thus explain reduced speed [18]. Additionally, it has been shown that increased levels of weight unloading lower the speed at which the energy expenditure of walking is minimal [19]. The unloading force reduces the amount of work that can be done against gravity, limiting the amount of energy that can be stored as gravitational energy. It has also been shown that weight unloading has a negative effect on posture and gait parameters such as stride length, speed and antigravity muscle activity [20]. Additionally, the nature of propulsion changes; because of the reduced GRF, people adopt a compensatory strategy to propel themselves forward which involves an abnormal degree of knee flexion during stance in order to pull the body forward [20].

---

[1] Besides storing energy in gravity or strain, it is also possible to store energy in fluid vorticity, as can be observed in fish or flying insects [11].

A possible solution that may ameliorate these problems – and thus make the rehabilitation more task-specific – is including a forward force with the vertical unloading force. One study by Mun *et al.* attempted to train the ankle plantar flexors, hip extensors and hip flexors using a robotic walker that applies a horizontal force at the hips [15]. Plantar flexor, hip extensor and hip flexor strength did improve, though during training the gait parameters were not preserved. Greater flexion on the ankle, knee, and hip joint could be observed. The constant drag that was applied mostly affected the stance phase, the swing phase was left unaffected. A second study by Gottschall *et al.* applied a horizontal assisting or impeding force and found this has a big effect on the anterior-posterior (AP) GRF [21]. The increase in AP GRF was much higher than the increase in applied horizontal force. This indicates that applying an external horizontal force might prevent BWS users from adopting a compensatory strategy to increase their AP GRF. Little research has been done into the effects of a combined forward and vertical unloading force during gait rehabilitation. One study by Mignardot *et al.* reports that the negative effects that BWS has on gait parameters can be alleviated with a well-calibrated forward force [20]. Whereas the results from Gottschall indicated that a forward force might prevent the compensatory strategy in terms of AP GRF, Mignardot shows that a forward force reduces the compensatory strategy in terms of stride length, speed, double stance duration and antigravity muscle activity, as well as the oscillations of the center of mass (CoM) of the user and the GRF profiles.

1.3. Need for Forward Force

The unloading force of a BWS system alters the kinetics and kinematics of walking, such as the GRF angle, speed, stride length and CoM oscillations. For task-specific motor learning it is preferred to assist the kinetics without changing the kinematics [9]. That is, reduce the magnitude of forces equally, such that, for example, the direction of the GRF vector over time is maintained. This is expected to maintain the kinematics and other spatiotemporal parameters of human gait [10].

Additionally, passive systems are likely to apply a backwards force on the user due to inertia and friction. Apte *et al.* [22] has shown that applying 0% BWU has a negative effect on gait parameters, compared to being disconnected from the unloading apparatus. This could be compensated with a forward force.

1.4. Patent: a Passive BWS Device for Forward Forces

1.4.1. Motivation

To investigate the effects of a horizontal propulsive force, and to expand the toolkit of therapists with limited budget, a passive, human-powered, gait-synced device was conceived [23].

Actively controlled systems, require accurate sensors to measure the motion of the users, sophisticated control algorithms to convert the sensor data into motor input, and powerful motors to generate forces at a high frequency. As a result, active robotic rehabilitation interfaces are often often unaffordable to all but the best-funded clinics. Compared to their active counterpart, the mechanisms of passive BWS systems are cheaper (they are purely mechanical), more reliable (they have fewer components) and they have better compatibility with electromagnetic fields and local power outlets (or lack thereof). They are also subject to more lenient compliance than active systems, making them less prone to compliance issues.

In addition to providing an affordable alternative to active robotic systems, possible new applications of a passive system include home use and use in 3rd world countries. A passive device can be constructed using inexpensive off-the-shelf components for home use or made from salvaged bicycle parts for use in a developing countries. This can greatly increase the availability of gait therapy, benefiting people all over the world.

Functionally, passive BWS systems are capable of providing a safe training environment and weight offloading. However, their friction, and to a lesser extent inertia, generate a backwards force on the user. While the advantages of a forward force in a BWS system are being investigated [20], a backwards force has a clear negative impact on gait rehabilitation [22].

Human-powered systems require additional effort from a user during an already-intensive training. The aim of the device was to make the harvesting of energy as unobtrusive as possible. One option is to use energy from muscles that are included in the training, such as leg of antigravity muscles, and another option is to use entirely different muscles:

- Walking muscles
  During walking energy is used to elevate the center of mass of the human body, after which is lowers again. Leg muscles generate energy to move the body up, storing energy as gravitational energy. When the body lowers this energy is released, after which some is converted to kinetic energy, and some is dissipated during the ground impact. Part of this gravitational energy might be harvested to power the forward propulsion of the device (and thus the human). An advantage of doing so would be that the propulsive action generated by the device (and thus indirectly generated by the human) is always in sync with the walking gait.

- Muscles unrelated to walking
  Walking is a complicated coordinated process and it might be beneficial to interfere with that as little as possible. Unloading weight and aiding the forward propulsion might be necessary for task-specific training, but harvesting energy from the walking process might interfere too much, potentially undoing the improvements of task-specificity that the forward force assistance brings. One option would be to have the human grip an hydraulic/pneumatic sack. Tightening the grip could be used to generate energy, the energy could be transferred using the air or oil, to be used elsewhere to generate the propulsive force.

Externally powered systems, on the other hand, assist the human without requiring additional effort from the human. They do require some initial effort from the physical therapist or other caregiver though, to store some energy in the system. Such energy may be stored as mechanical potential energy:

- Counterweight
  A counterweight may be suspended from the end of the rail, and connected to the pulley. A transmission will be required for the rail length is longer than the rail height height. A counterweight would not be a local solution, it requires components over the entire length of the rails. It will be difficult to change direction and even when standing still a forward force will be applied.

- Constant torque spring
  A constant torque spring may be connected to the wheels of the pulley to provide a constant forward force. Additionally, a transmission may be required to match the force-length characteristics of the spring to the human needs.

Continuously having to 'reload' the system with energy, and having to resist a forward force during idle standing render the externally powered systems impractical. Systems powered by muscles unrelated to walking may require additional coordination from the human to sync the power generation with their gait, increasing the mental load of a challenging task even further. In order to make the device as intuitive as possible it will be powered using the user's walking muscles.

1.4.2. Working Principle

The device has three basic functions: unloading body weight, handling falls and enabling forward locomotion. Unloading weight is accomplished by using an elongated spring and falls are prevented by limiting the elongation of the spring. Enabling forward locomotion is accomplished by using a ratchet to convert the bidirectional vertical oscillations that naturally occur during gait to unidirectional forward motion of the pulley.

By switching the free direction of the ratchet the device can switch between converting either the up or the down stroke of vertical oscillations into forward motion. The other motion will roll freely on the ratchet and not produce motion of the pulley. The freewheel that produces the forward motion of the pulley does not prevent the pulley from moving faster than the motion induced by the vertical oscillations. Though in that case, no propulsive force will be transmitted.

The patent [23] entails multiple embodiments of this working principle, as shown in Figure 1.2. Both embodiments connects to a slingbar that connects to the user via a harness.

The two embodiments share the same working principle but have different implications for the physical design. In the single-axle embodiment the ratchet has to radially carry the forces from falls and weight unloading. In the elongated embodiment the weight of the user is carried by the bearings in the wheel axles, only a fraction of the weight loads the ratchet.

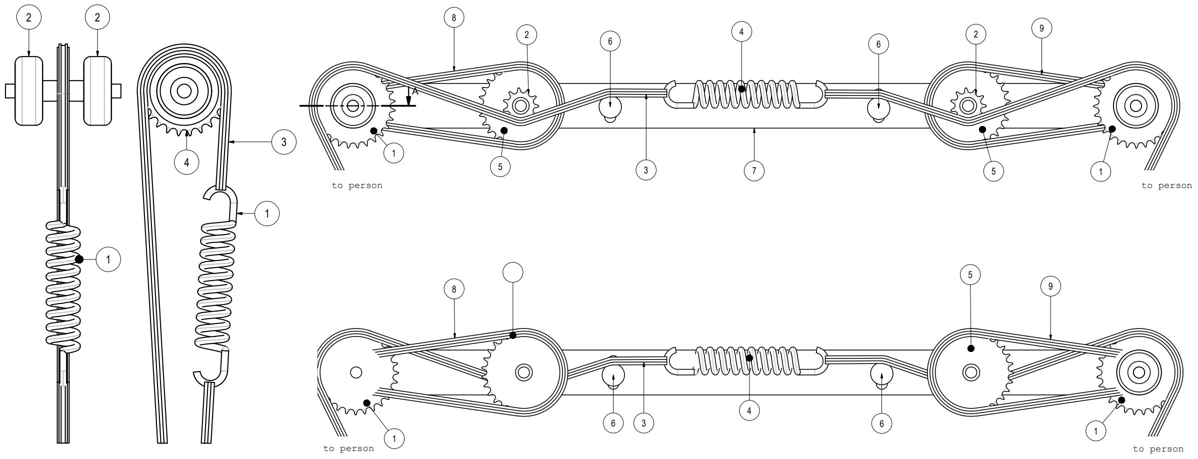

(a) Single-axle embodiment.

(b) Elongated embodiment.

Figure 1.2: Two embodiments of the patent. Both embodiments end in a single suspension point that connects to the user. This point lies below both figures. Figure (a) shows the single-axle embodiment. The spring (1) is connected to the chain (3), which is routed over the sprocket (4). The sprocket is connected to the wheels (2) via the ratchet. Figure (b) shows the elongated embodiment. Again, the chain (3) is connected to the spring (4). The chain is supported by sprockets (1) which can rotate freely with respect to the wheels. The ratchets are located between sprockets (2) and sprocket (5). Sprocket (5) drives a secondary chain which is connected to the wheels. Images from [23].

This thesis will treat the single-axle embodiment. It is the simplest embodiment that still preserves the main working principle. Maybe it will turn out, after this thesis, that additional functionality may be required. In that case, research can continue with the elongated embodiment. For now, however, there is no reason to justify additional complexity.

Figures 1.3 and 1.4 detail the working principle of the single-axle embodiment, hereafter named ’the device’. Figure 1.3 shows the isolated behavior of the device. When the end-effector idles, the device does too. Moving down does not elicit a response from the pulley, but moving up does. When the end-effector is already moving forward at a sufficient pace, moving the end-effector up may not elicit a response from the device. Critical here is the slope of the end-effector trajectory with respect to the rail.

The device will be coupled to a user, rather than be used in isolation. If the trajectory of the human has a sufficiently steep slope it will elicit a response from the system and receive a forward force. Figure 1.4 shows the behavior of the device when coupled to a human. When the user moves up, the pulley moves ahead of the user and the spring and chain are at an angle. The unloading force is now also at an angle and thus contains a horizontal component.

1.5. Contributions of this Thesis

Before the start of this thesis, the working principle of the patent has been described in only vague qualitative terms; a prototype has neither been designed nor constructed, and the operating principles have not been validated on a physical system. This thesis will quantify the operating principle, simulate the interaction with human gait and construct a prototype. All this will be done for the single-axle variant presented in the patent.

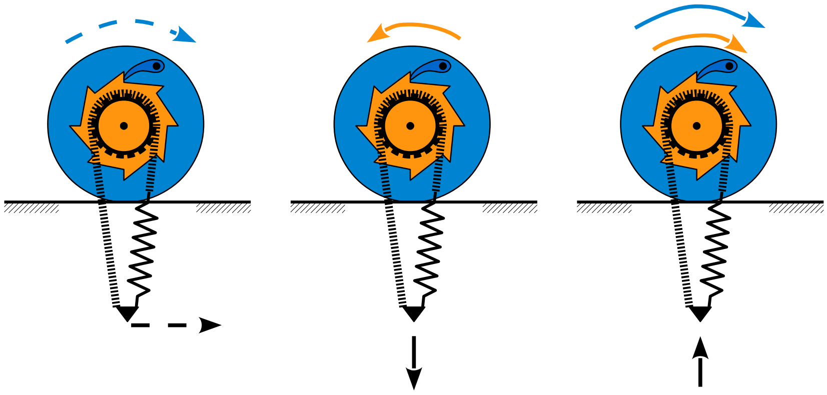

Figure 1.3: Working principle of the device. The wheels, shown in blue, roll on the rails. The sprocket, shown in orange, is connected to the wheel using a ratchet, allowing it to rotate relative to the wheel in one direction. A chain is routed over the sprocket. One end connects directly to the end-effector while the other end connects to the end-effector via an elastic element. Left: When the end-effector idles, the device idles as well. When the end-effector moves forward the blue wheel will roll and the device will follow. The sprocket remains stationary. Middle: When the end-effector is moved down, the spring will elongate and the chain will make the sprocket rotate counter-clockwise. The ratchet does not engage in this direction so the wheel remains stationary. Right: When the end-effector moves up the spring and chain will make the sprocket roll clockwise. This engages the ratchet, causing the wheel to rotate in tandem with the sprocket, making the wheel roll forward.

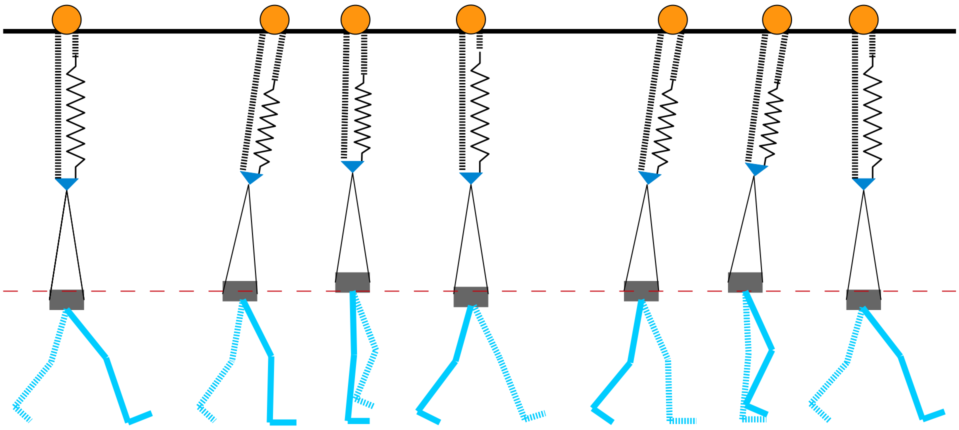

Figure 1.4: Working principle of the device with a human. During a gait cycle humans moves up and down. At the left in the figure the user starts in the low double-stance, right foot forward. From here on, the user pushes off with his off with his left foot and vaults over his right leg. During this motion the user moves upwards, triggering the ratcheting mechanism in the device. The user will make the pulley roll forward. Now that the pulley is no longer right above the user, the force will no longer be solely vertical. The is now a horizontal force component present, caused by the unloading force acting at an angle. Once the user's vertical velocity decreases, the ratcheting mechanism of the pulley releases and the device returns to its position right above the user.

2

Theoretical Concept Realization

2.1. Static Analysis

2.1.1. Introduction

The device can be regarded as an input-output device. The trajectory of the end-effector will serve as input and the output will be the force exerted on the end-effector. This section will set up a static model of the ratcheting pulley. For an arbitrary but stationary end-effector position the force of the end-effector can be computed. In this section the end-effector position, relative to the pulley, is determined by the length l and the angle θ, depicted in Figure 2.1.

The model consist of 3 bodies, all connected to one another. Figure 2.1 shows the bodies and gives some dimensions. The wheel is shown in blue, the sprocket is shown in orange and the end effector is labeled E. The wheel rolls on a fixed rail, the sprocket is hinged to the wheel in point O with a ratchet and the end-effector is coupled to the sprocket by a chain and a spring. This static analysis excludes inertia, and instead focuses on the kinematic relation between the end-effector and the pulley. For this reason the slip between the wheel and rail will be assumed to be perfect, the spring to be linear and the ratchet to be backlash-, friction- and slip-free.

The wheel has a radius r_w, the sprocket has a radius r_s. The spring elongation from rest s is related to the total length l via a transmission ratio of 2 (meaning 1 unit of end-effector translation will result in 2 units of spring extension) and via a constant offset K which is equal to the rest-length between the pulley center and the end-effector. The rest-length is defined by the rest length of the spring, the length of the chain and the length of straps and cables connecting the user to the pulley.

$$s = 2(l - K) \quad \forall\, l \geq K \tag{2.1}$$

2.1.2. Methods: Free-body Diagram

Using the method of sections, the forces in the device can be revealed. Figure 2.2 shows the sectioned device and the forces. F_p is the external force applied at the end-effector. F_c is the force in the chain that directly connects the end-effector and sprocket, and F_s is the force in the spring. These three forces are parallel and operate at an angle θ. F_u is the vertical force between the rail and the pulley, F_f is the horizontal force between the pulley and the rail.

Using Figure 2.2 the equations of equilibrium can be derived. In the right figure the force equilibria in x and y direction, as well as the moment equilibrium around point C can be derived:

$$\sum F_x = 0 \quad \Leftrightarrow \quad F_\mathrm{f} = \sin\theta(F_\mathrm{c} + F_\mathrm{s}) \tag{2.2}$$

$$\sum F_y = 0 \quad \Leftrightarrow \quad F_\mathrm{u} = \cos\theta(F_\mathrm{c} + F_\mathrm{s}) \tag{2.3}$$

$$\sum M_C = 0 \quad \Leftrightarrow \quad F_\mathrm{s}(r_\mathrm{s} - r_\mathrm{w}\sin\theta) = F_\mathrm{c}(r_\mathrm{s} + r_\mathrm{w}\sin\theta) \tag{2.4}$$

In the left figure the force equilibrium along an angle θ can be derived.

$$\sum F_\theta = 0 \quad \Leftrightarrow \quad F_\mathrm{p} = F_\mathrm{c} + F_\mathrm{s} \tag{2.5}$$

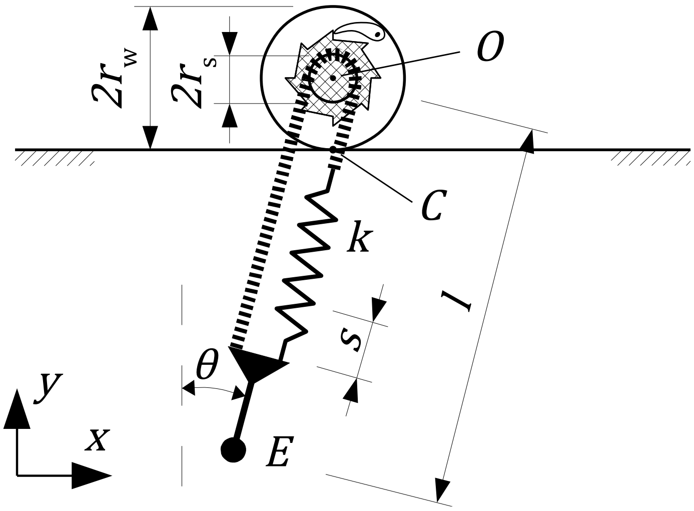

Figure 2.1: Schematic overview of the simple prototype, including relevant dimensions.

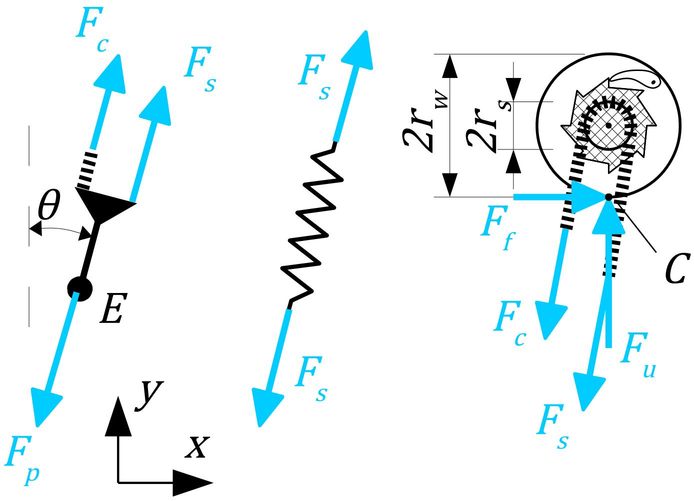

Figure 2.2: Free-body diagram of the simple prototype. For simplicity, F_c and F_s are assumed to be parallel.

Furthermore, the spring force F_s is defined by the elongation of the spring s.

$$F_\mathrm{s} = ks = k2(l - K) \quad \forall l \geq K \tag{2.6}$$

In these 5 equations the inputs, l and θ, are given, and the parameters, k, r_w, r_s, and K, are known. There are 5 unknown forces remaining, making the system statically determinate. This means each force can be uniquely solved.

When the pulley is behind the user, the spring will simply pull the pulley forward, therefore in the static case, θ cannot be smaller than 0. Similarly, θ will not be larger than $\frac{\pi}{2}$ because the user would need to coincide with the support rails, which is not possible.

$$\frac{\pi}{2} > \theta \geq 0 \tag{2.7}$$

All the forces are bounded as well. F_c, F_s and F_p describe the force of an element which cannot be compressed, and therefore cannot be negative. F_u is a contact force and can therefore not be negative. F_f can only be negative when $\theta < 0$, or when $F_\mathrm{c} + F_\mathrm{s}$ becomes negative, both of which are not possible.

$$F_\mathrm{c}, F_\mathrm{s}, F_\mathrm{u}, F_\mathrm{f}, F_\mathrm{p} \geq 0 \tag{2.8}$$

Between the pulley and the rails is Coulomb friction:

$$F_\mathrm{f} \leq \mu F_\mathrm{u} \tag{2.9}$$

From equations 2.3 and 2.2 and inequalities 2.9 and 2.8, it can be found that:

$$\theta \leq \tan^{-1} \mu \tag{2.10}$$

Physically, this means the unloading force vector should lie within the come of friction. From equation 2.4 and inequality 2.8, it can be found that:

$$\theta \leq \sin^{-1} \frac{r_s}{r_w} \tag{2.11}$$

when $r_w \geq r_s$. This last relation can also be interpreted from the moment equilibrium around point C. When θ increases, the lever arm of F_c increases and the lever arm of F_s decreases. For $\theta = \sin^{-1} \frac{r_s}{r_w}$ the lever arm of F_s equals zero, and for moment equilibrium F_c needs to be zero as well. For larger θ, F_c would need to be negative to maintain the moment equilibrium. The ratio of the radii will be put in a new parameter:

$$R = \frac{r_w}{r_s} \tag{2.12}$$

which means the maximum achievable angle can be written in terms of this new parameter:

$$\theta \leq \sin^{-1} \frac{1}{R} \tag{2.13}$$

Additionally, R represents the upper bound of the transmission i between the end-effector height and the horizontal pulley translation. When the end-effector is below the pulley and moves up by an infinitesimally small distance d_{in}, the sprocket rotates $\psi = d_{\text{in}}/r_{\text{s}}$ radians. This engages the ratchet, so the wheel will rotate as much as the sprocket. The wheel will roll on the rails, translating $d_{\text{out}} = r_{\text{w}}\psi$. The transmission ratio then becomes $i = \frac{d_{\text{out}}}{d_{\text{in}}} = \frac{r_w}{r_s} = R$.

As soon as the end-effector is longer directly below the pulley, the transmission ratio is slightly altered. When the end-effector moves up, only the component of the displacement that points towards the pulley will make the sprocket rotate. The sprocket rotation will now be lower, as will the pulley translation. Thus the transmission ratio will also be lower.

2.1.3. Results

The device depends on tension in all chains to operate. This requirement puts a limitation on the maximum input angle. The unloading force always operates at this angle, which means the vertical and forward unloading force will be coupled by this same angle. Therefore, the parameter R, together with the maximum unloading force determines the maximum forward force.

2.1.4. Discussion

The unloading force of the device can be tuned using the rest length K and the spring stiffness k. The spring stiffness is amplified by the transmission ratio between the spring elongation and the total device elongation.

The perceived stiffness at the end-effector will be $2^2 = 4$ times as high as k. The transmission ratio acts once when translating the end-effector displacement to the spring elongation, and acts again when the spring force is translated back to end-effector force.

This static analysis disregarded inertia and found a minimum and maximum value for θ. In a more realistic model, the range of θ will be slightly higher. Inertia may cause θ to be slightly smaller than 0, as well as cause it to be slightly larger than the maximum imposed by R. This will be temporarily though, the pulley will quickly roll back to the predicted minimum or maximum. How quickly it will do so depends on the inertia of the pulley (the lower, the faster). A pulley with large R will generally have large r_w (r_s will have a minimum, as will be shown later on) and consequently a large inertia.

A high R means little vertical movement of the end-effector will result in a lot of horizontal motion of the pulley, however the horizontal movement of the pulley is capped early on because the maximum θ is reached. A small R means relatively little horizontal motion of the pulley, yet it will be capped relatively late. This presents a conflict, a high maximum angle (and resulting high forward force) requires a lot R, meaning that it will take long to reach the maximum angle, if at all.

It is likely there is an optimum somewhere in the middle. For example, Mignardot [20] reports an forward force that is equal to 10% of the unloading force as optimal, meaning a force angle of $\tan^{-1}(0.1) = 5.7\,\text{deg}$. Being able to achieve this angle would require $R \leq 10$. This finding does not completely generalize to this device though, for their forward force is constant and this device's forward force gradually grows to its maximum as the user moves up and θ increases.

Determining if a certain walking pattern will actually provide sufficient motion at the end-effector such that the pulley reaches the maximum angle is no trivial task. Upwards motion of the end-effector leads to forward motion of the pulley. The forward motion of the pulley relative to the end-effector and the vertical distance between the end-effector and the pulley ultimately determine the angle. Furthermore, as the angle deviates from 0, vertical motion of the end-effector is no longer completely translated to horizontal pulley motion because of nonlinearities. The dynamic analysis in the next section aims to properly capture this behaviour.

2.2. Dynamic Analysis: Combination with SLIP Model

2.2.1. Introduction

This section will set up a dynamic model of the device. Both the trajectory and the force of the end-effector will now be a function of time. An explicit relation between the input and output might exist, but for convenience a numerical simulation is used. The system is not linear, and depends on both the current and the past input.

During use as intended, the device will be connected to the user. The movements of the user will excite the device and cause a reaction force at the end-effector. The force will influence the gait of the user, and thus the input of the device This interaction is the primary interest of this section as well as this thesis.

In order to simulate this interaction, a numerical model of the device will be coupled to a numerical model of human gait; the SLIP model [24]. Out of a number of gait model, the SLIP model is the most suitable for modeling BWU [25]. Figure 2.3 shows the SLIP model.

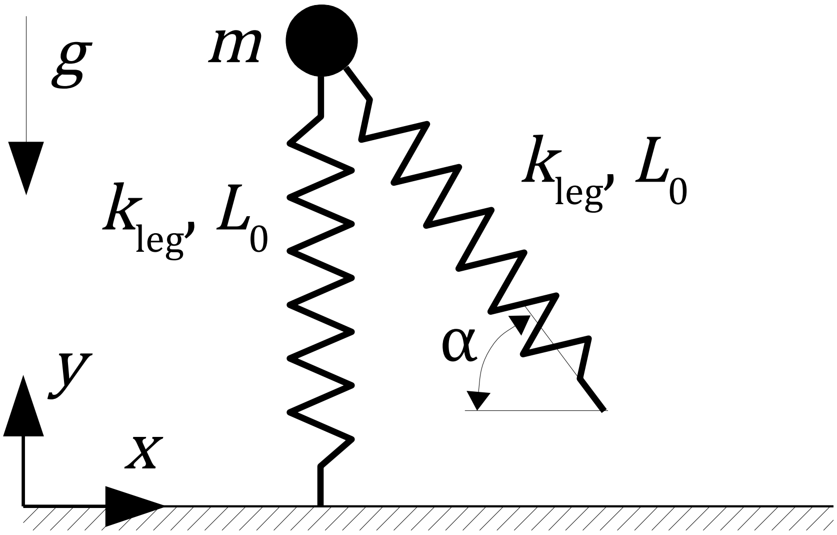

Figure 2.3: Overview of the SLIP model. It consists of a single mass m that represents the human body and two massless linear springs that represent the legs. The springs have equal spring stiffness k and rest length L_0 and only affect the model dynamics during stance phase. In swing phase the front leg is held at angle α to determine when and where the front foot will touch the ground. When it does, it attaches to the ground. When the springs elongate more than their rest length they disengage from the ground.

As the device connects to a human, it will also connect to what represents the human in the SLIP model, the mass.

2.2.2. Methods: Numerical Simulation

Figure 2.4 shows the combined model and its parameters. We will use the following set of generalized coordinates $\boldsymbol{q}$ to compute the equations of motion using Euler-Lagrange:

$$\boldsymbol{q} = \begin{pmatrix} \phi_\mathrm{w} \\ \phi_\mathrm{s} \\ x_\mathrm{b} \\ y_\mathrm{b} \end{pmatrix} \tag{2.14}$$

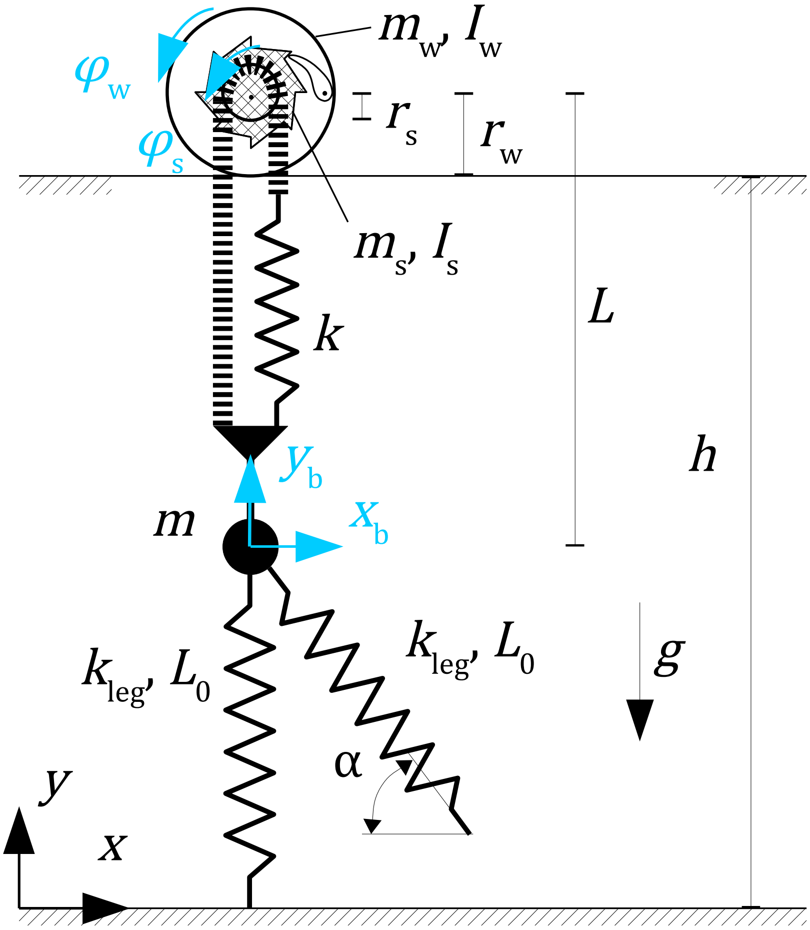

Figure 2.4: Overview of the combined model of the device and the SLIP model.

The ratchet has two states: it is either engaged or disengaged. The SLIP model has three states: single-leg support, double-leg support and no-leg support. The chain on the left side has two states: slack or taut. The chain on the right side (connecting the spring and sprocket) also has two states: slack or taut. Modeling all states would give rise to $2 \cdot 3 \cdot 2 \cdot 2 = 24$ different sets of equations of motion, and 24 different event functions to switch between them. Furthermore, many of those event functions will have to be accompanied by impact functions.

The no-leg flight state of the SLIP model will be removed, for this thesis is limited to walking gait, not running gait. The slack state of the spring-chain will be removed. This state will only occur if the pulley moves far ahead of the human, a situation that is highly unlikely to occur. The slack and taut state of the left chain stay, for they are required to prevent the pulley from going past θ_{max}. However, it will not be modeled as two separate states, rather a one-sided controller will be implemented to ensure the constraint only pulls and does not push. This leaves us with 2 SLIP model states, and 2 ratchet states, totaling 4 states. These 4 states including 4 event function (note there are now no impacts left) will be modeled in MATLAB (MATLAB Release 2017a, The MathWorks, Inc., Natick, Massachusetts, United States). Details on the implementation can be found in Appendix A.

The simulations are run using the stiff `ode15s` solver. The need for a stiff solver mainly comes from the slack-chain constraint. The equations obtained from Euler-Lagrange are ordinary differential equations which could be solved using a non-stiff solver, but when we expand them with the algebraic constraint equation from the ratchet then the set of equations become differential and algebraic equations (DAE). DAE are best solved using stiff solvers, particularly `ode15s` [26].

The initial conditions will be slightly different from the SLIP model. The original SLIP model features some pretension in the legs, though this will lead to problems when incorporated in our model. The pretension force in the legs and the weight-unloading force of the device may total more than the weight of the body, causing it to accelerate upwards from midstance, rather than downwards. This is undesired and therefore there will be no pretension in the legs.

This means, however, that the triplets of leg stiffness k_{leg}, angle of attack α and initial horizontal velocity of the point mass v_0 of the original SLIP paper will not produce a stable limit cycle in this model. In order to find a new triplet, the leg stiffness and angle of attack will be kept identical. Those are assumed to be neurological control parameters of human gait, so a new initial velocity will be found. The initial velocity that produces the most stable gait (meaning the smallest difference in begin and end velocity after 1 gait cycle, from midstance to midstance) will be used. This velocity and the other parameters are reported in table 2.1.

Furthermore, other relevant physical properties and initial conditions are also reported in table 2.1. The SLIP model starts in midstance, with horizontal velocity v_0. The pulley starts right above the mass of the SLIP model, and provides the specified amount of body weight unloading (BWU) at the starting position.

Table 2.1: Properties used for simulating the combined model of the device and SLIP model.

Property	Value	Units
α	69	°
k_{leg}	14000	N/m
L_0	1	m
v_0	1.155	m/s
R	0.25...10	(-)
BWU	0...70	%Bodyweight
m	80	kg
h	2.4	m
r_s	0.03	m
r_w	Rr_s	m
m_s	0.375	kg
m_w	$254.473r_w^2$	kg
I_s	$\frac{1}{2}m_s r_s^2$	kgm^2
I_w	$\frac{1}{2}m_w r_w^2$	kgm^2
g	9.81	ms^{-2}

The simulation runs various BWU and R values for 10 seconds. If the model completes these 10 seconds the run is deemed stable; if it fails it is unstable. Failure is determined from either a negative horizontal velocity of the mass, or extension of the leg springs beyond their rest length. From the stable runs various gait parameters are recorded such as the average stride length, average horizontal velocity of the mass and vertical excursion of the mass.

2.2.3. Results

Figure 2.5a through 2.5c show the results from the simulations under various conditions. In all figures a clear distinction at $R \approx 2$ can be observed, where the results seem to rapidly deviate. Inspection of the simulation data indicates that this is the transition point between the device actively helping the SLIP model propel forward (ratchet engagement) or not (no ratchet engagement). For smaller R the device does not aid in forward propulsion and simply functions as a vertical BWS trolley. For larger R it actually propels the user forward. When the device aids in forward propulsion, it will be referenced to as 'active', when it does not it will be referenced to as 'inactive'.

The activation threshold runs approximately from R=1.5 at BWU=0 to R=3 at BWU=0.5. Figure 2.5b shows that BWU decreases the average height difference and Figure 2.5c shows that BWU increases the average step size. Both the decreased height difference and the increased average step size reduce the slope of the trajectory. This causes the device activation threshold to increase with BWU.

The contours are not completely smooth. At high BWU and R the contours become discontinuous, and at random locations in the plots the contours may briefly deviate from the general trend. See, for example, Figure 2.5b at BWU=0.3 and R=0.25, or BWU=0.25 and R=6 in Figures 2.5b and 2.5c. This is caused by the SLIP model being very sensitive to perturbations. In the original article a 3D plot shows which combinations of k, v_0 and α produce a stable gait. The stable walking domain is very narrow so in terms of Euclidean distance, instability is never far away.

In figure 2.5a the average horizontal velocity of the mass is shown. When the device is inactive, increased BWU leads to decreased velocity. This is known from literature [17, 18]. In the active region the device can either increase of decrease the average walking speed. For BWU between 0 and 0.3 and R between 2 and 6 the average speed increased. Outside this region it is decreased. At the border between those regions (countour line 1.195) the average walking speed is unchanged.

In figure 2.5b the average height difference of the mass is shown. When the device is inactive, increased BWU leads to decreased average height difference. Comparing arbitrary BWU levels, the average height difference in the active region is even lower than in the inactive region.

In figure 2.5c the average step size of the mass is shown. When the device is inactive, increased BWU leads to an increased step size. Comparing the active and inactive state for an arbitrary BWU level shows that the active device increases the step size even further, except for very large R, where the step size is unchanged.

2.2.4. Discussion

Walking is a constant interplay between potential and kinetic energy. BWU is known to perturb this relation and and the hypothesis was that our device will somehow reduce this perturbation.

The gait deterioration due to BWU is evident. For the average velocity the deterioration starts slowly and starts gradually deteriorating from 25% BWU, whereas the average height difference and average step length deteriorate linearly with the amount of BWU.

At very specific configurations the device can ameliorate the average velocity deteriorations that occur due to BWU. In figure 2.5a the average speed at 0% BWU lies between 1.19 and 1.195 m/s. For BWU of up to 30% there is a small region where the average velocity is equal to the baseline velocity. This would require a different R value for every BWU condition though. As the region is very narrow it is also very sensitive to misconfigurations of the amount of BWU or R.

Outside the aforementioned region of Figure 2.5a, and in the complete active domains of figure 2.5b and 2.5c the values of the gait parameters are deteriorated even further.

The device has a positive effect on the stability of the SLIP model. Increasing BWU up to ≈45% causes the model to become unstable and fail. An R value between 3.5 and 4 seems to make the model stable up to ≈55% BWU. It is unknown, however, how this would translate to human gait. The SLIP model assumes static neurological control. In reality, humans may slightly adapt their neurological control strategy to combat instabilities.

When our device activates, the interplay between potential and kinetic energy is altered. The height variation is reduced, and thus the potential energy. The system is conservative so this energy will lead to an increase in kinetic energy, which equals an increase in velocity.

There is no 'one size fits all' R value. The ratio R matters little for the average step size, as long as it is larger than the device activation threshold For the speed and height difference the contour lines seem to be mostly diagonal, indicating every BWU condition requires a different R.

An alternative walking model to combine with could be the virtual pivot point (VPP) model [27]. The VPP model extends the SLIP model with a trunk that is controlled using a hip torque. Compared to the SLIP model, the VPP model can be used to predict trunk movements and hip torques during human walking. The hip torques, and their reaction force on the ground, provide more accurate GRF data than the SLIP model. The trunk motion is not of primary interest but the GRF might be an interesting additional metric and may be a candidate for future research.

Nonetheless, the SLIP model is the simplest model that provides in the needs. Those needs are a trajectory that serves as input for the model, and the ability to be influenced by external forces.

The SLIP model was suitable for simulating the energetics of walking and the influence of our device on this. The conservative SLIP model couples well with the conservative model of our device. The only real drawback is that the conservative model can not include friction. Sliding friction will likely be the largest cause of difference between the model and the reality of the device. Friction is expected to deteriorate the gait parameters even more.

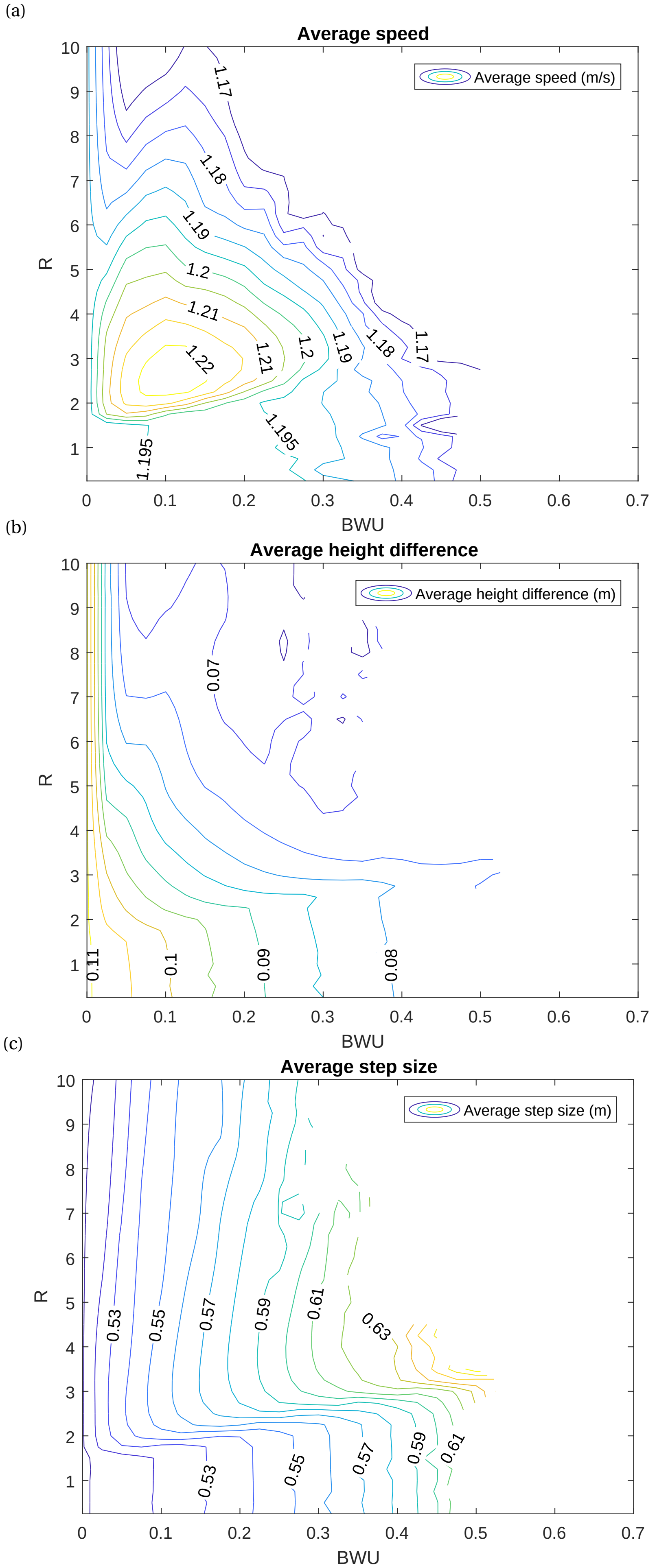

Figure 2.5: Contour plots of (a) the average horizontal velocity, (b) the average height difference of the body mass between midstance and symmetrical doublestance and (c) the average step length of our combined model, under the influence of various BWU and *R*.

3

Mechanical Concept Realization

3.1. Introduction: Design Requirements

3.1.1. Functional objectives

Based on the previous simulations, the design variables of interest are:

- *R*
  Prototypes with various *R* allow uw to investigate which value best improves gait parameters. Multiple prototypes with *R* of 2, 4, 6 and 8 are constructed. An even higher *R* would result in prototypes that are too large and heavy to be practical.

- Unloading
  A slightly unloaded spring will provide the unloading (and forward) force. The spring stiffness will be chosen such that the eigenfrequency of the unloaded mass suspended by the spring will be equal or higher to the stepping frequency of the user. There will be multiple users so the device must be able to accommodate multiple springs.

- Vertical amplitude/spring elongation
  The end-effector is connected to the user and should be able to accommodate the vertical motion of the user. This amplitude is transferred to the spring, in addition to the already present static unloading elongation. The spring should be able to accommodate a vertical peak-to-peak amplitude of 0.1m.

3.1.2. Safety objectives

Device should be able to withstand a certain peak force without endangering the user. The reference design mass is 80kg. Later generations of the prototype can focus on further optimizing the strength of the device. Because of the spring, falls will be dynamic. In a dynamic fall the user is softly caught by the spring, meaning the peak mass will be twice the reference mass. Thus for safety calculations, a maximum mass of 160kg will be used.

3.1.3. Wish List

The following variables will also influence the device's functionality

- Low inertia
  Inertia increases the undesired interaction forces with the user.

- Low friction
  Friction creates an undesired backwards interaction force with the user.

These undesired interaction forces counteract the functionality of the device, which is provide certain desired interaction forces.

3.1.4. Safety Factors

The international[1], European[2] and Dutch[3] norm NEN-EN-IEC 60601-1 specifies safety factors (SF) for medical equipment. Table 21 of this norm specifies SFs for support systems. Because we will be using ductile materials (specific elongation at break equal to or greater than 5%), a SF of 2.5-4 is prescribed. Being in the lower or the higher end of the SF range is determined by how accurately the external forces are known and quantified.

3.2. Methods: Component & Material Selection

Figure 3.1 highlights the various components that were be designed or purchased. The slingbar and harness are bought off-the-shelf and will not be treated in this report. In the 4 prototypes that are built, all components are present, though the wheel and flange sizes vary to realize different R.

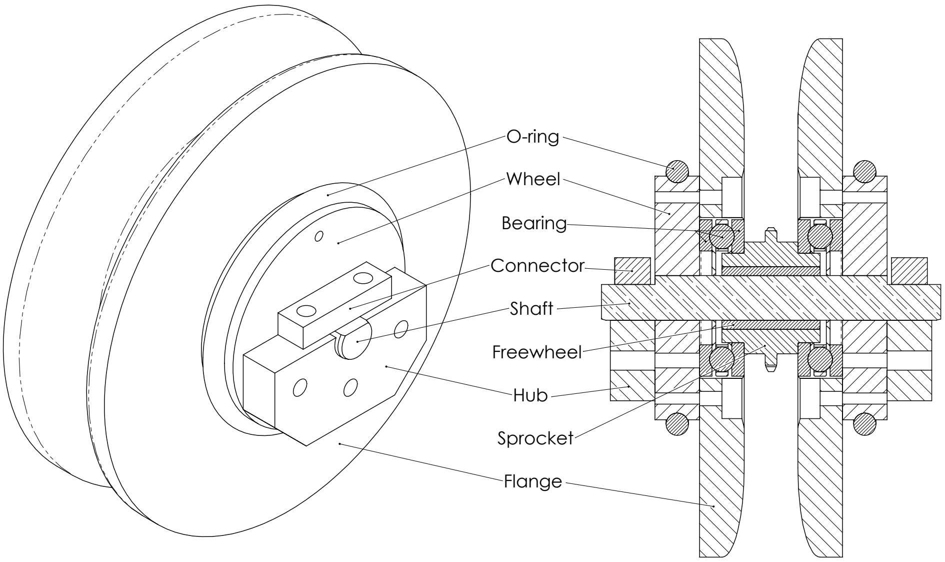

Figure 3.1: Overview of the pulley, indicating the different components. The O-rings run on the rails, which are not shown. The flanges fit in the gap between the rails.

3.2.1. Wheel & Flange

The wheels run on an overhead rails. If the wheels would not be stabilized, the wheels may deviate from the rails and drive the the chain into the rail. Because this would be detrimental to the functioning of the device this will have to be stopped. Flanges are used to stabilize the wheels in the rails. The four points of contact between the two flanges and the rails span a rectangle, as shown in Figure 3.2. For stability, the aspect ratio of this rectangle will be 1:3. That is:

$$\frac{l}{w} = 3 \tag{3.1}$$

Where w is the width of the gap between the rails. Together, the wheel radius r_w and the flange radius r_f determine the length of the rectangle:

$$l = 2\sqrt{r_\mathrm{f}^2 - r_\mathrm{w}^2} \tag{3.2}$$

Each prototype will operate in the same rails, so for identical stability all rectangle sizes will be identical. but the wheel size will be different. Therefore the distance that the flange extends over wheel will decrease for larger wheel sizes. While the outside of the flanges serves to support the device in the rails, the inside of the flanges serves to support the chain, making sure it slides as smoothly and silently as possible. In order to fulfill these demands, the flanges will be made out of nylon (PA6).

---

[1] IEC = International Electrotechnical Commission

[2] EN = European Norm

[3] NEN = 'NEderlandse Norm', Dutch norm

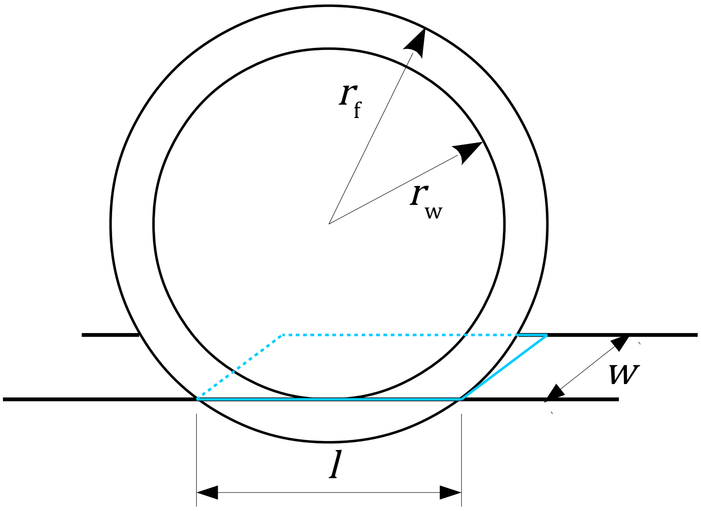

Figure 3.2: The contact points between the flanges and the rails span a rectangle. For clarity, only one wheel and flange are shown.

3.2.2. O-ring

O-rings are mounted on the edge of the wheels to ensure they do not slip on the rails. There is little literature on using O-rings this way. A closely related application is using O-rings as a low-power transmission belt between two not-necessarily parallel axes. For this application, the Parker O-ring Handbook [28] reports an initial pretension of 8-12%. Unlike the drive belt application, the radius of the rim of the wheel will be made slightly smaller than the radius of the O-ring cross-section. This secures the O-rings on the wheels and aids the flanges in minimizing the lateral movement of the pulley.

Suitable materials at the supplier are NBR and EPDM rubber. Both have excellent wear and creep properties, but NBR is available in a higher hardness and in much more sizes. Therefore the material of the wheels will be NBR.

3.2.3. Chain

The spring is suspended over the sprocket, one side attaches to the end-effector, the other side attaches to a spring. In the vertical position, the weight of the user is equally shared between the left and right side of the chain. Each side carries half the weight of the user in case of a dynamic fall, $0.5 \cdot 160\text{kg} \cdot 9.81\text{ms}^{-2} \approx 800\text{N}$. In order to fit between the flanges, the smallest chain that meets this specification is employed: No. 04, 6mm pitch chain (ISO 606/DIN 8187-1). This chain has a tensile strength of 3000N, giving a safety factor of $S_{\text{chain}} = \frac{3000}{800} = 3.75$.

3.2.4. Sprocket

The sprocket transmits power from the chain to the freewheel. To do so effectively, sprockets need about 16 teeth minimum [29]. The benefit of choosing a small pitch chain means 16 teeth will form a relatively small sprocket. Remember, to vary R, the ratio between the wheel and sprocket radius is varied. For a lightweight design, it is trivial to keep both radii small. Therefore a small sprocket and small-pitch chain will be used.

The sprocket is press fit onto the freewheel. To maintain the fit a minimum wall thickness of 3mm is required. The resulting outer diamter allows just enough space for 16 teeth. The pitch radius, which is used together with R to compute the wheel radius, is 30.75mm. For weight and machinability, the sprocket will be constructed out of aluminium.

3.2.5. Freewheel

The weight of the user is transferred through the sprocket, and reaches the freewheel as a radial load. The freewheel (HFL1022) has built-in needle bearings which have a dynamic load rating of 4650N. Dividing by the required load yields the safety factor: $S_{\text{freewheel}} = \frac{4650}{1600} = 2.9$.

3.2.6. Spring

The effective spring stiffness is chosen in such a way that the unloaded mass of the user resonating in the spring has the same eigenfrequency as the frequency of stepping of the user, which is assumed to be 1.6 steps/s.

The effective spring stiffness is not equal to the actual spring stiffness. Earlier, it was explained that there is a transmission ratio between the elongation of the spring and the displacement of the end-effector. This transmission ratio was equal to 2. For stiffness, this transmission ratio is squared, meaning the effective spring stiffness, as felt by pulling on the end-effector, will be 4 times as stiff as the spring in isolated conditions.

A range of springs is employed, and they can be easily interchanged. This allows for various amounts of weight unloading within the same device. A rope is employed parallel to the springs, ensuring the springs do not overextend and break.

3.3. Results

Technical drawings are located in appendix C. Figure 3.3 shows two photographs of the prototypes.

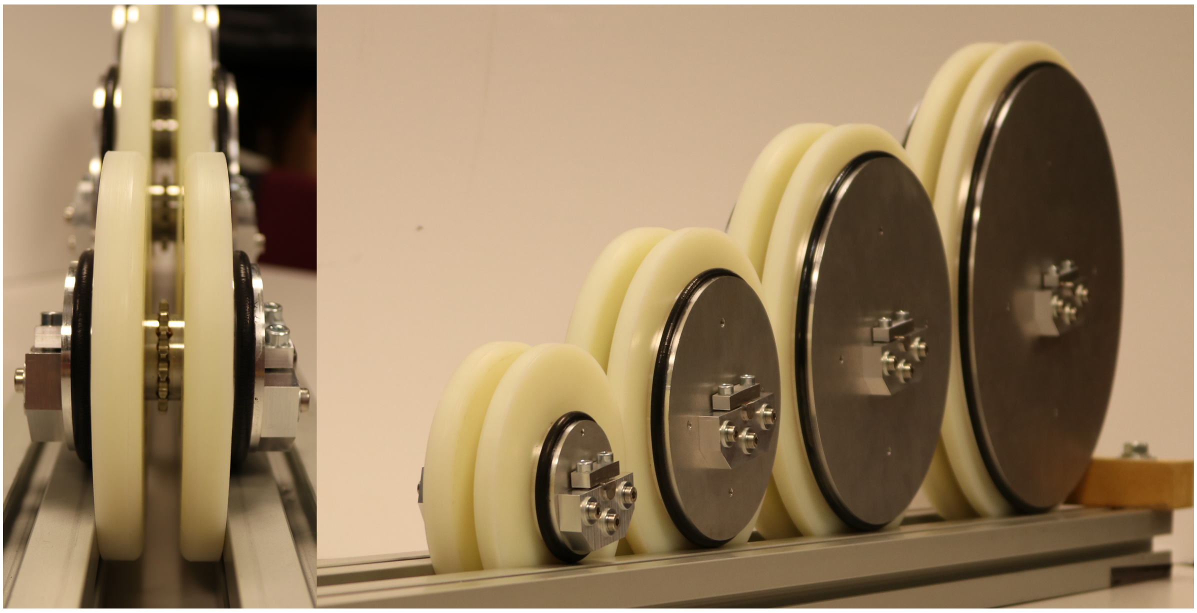

Figure 3.3: Photographs of the prototypes. Notice how the smaller prototypes have relatively large flanges.

Table 3.1 shows the properties of the prototypes. Sprocket and wheel values are shown separately. Each prototype consists of the same sprocket, with different wheels.

In subsection 2.1.2 a minimally required μ was found: $\theta \leq \tan^{-1}\mu$. By putting each of the prototypes in the rail and pulling on them with a chain this requirement could easily be validated. The angle at which the force pulled on the pulleys was gradually increased until one of the chains went past the contact point (meaning the other chain went slack) and the wheels started rolling. From this it can be concluded that $\mu > \tan\theta$.

3.4. Discussion

Design simplicity was ensured by keeping the number of parts low. The shaft and sprocket are both monolithic and the freewheel consists of a single purchased part. Each wheel consists of 5 parts, though this is mainly caused by the need for different materials. The outer rings of the wheel are made of rubber to ensure maximum grip, whereas the flanges are made out of nylon to minimize the friction. This conflicting design requirement prevents the wheel from being monolithic. The plate, hub and connector are made out of aluminium because of the strength and stiffness it provides. Making them out of nylon might have been possible, though this would have skyrocketed the dimensions and costs. The hub and plate might have been monolithic, but this would require milling away (=wasting) a lot of material. The connector and hub might have been completely omitted by using a press-fit between the wheels and the shaft. This would pose difficulties

Table 3.1: Prototype properties. Values for the sprocket and the various wheel sizes are shown separately. Each prototype consists of a sprocket and one wheel size.

R	Property	Value	Units
(-)	r_s	0.015375	m
	m_s	0.375	kg
	I_s	0.000049	kgm^2
2	r_w	0.03075	m
	m_w	0.6160	kg
	I_w	0.0001	kgm^2
4	r_w	0.0615	m
	m_w	1.3378	kg
	I_w	0.0016	kgm^2
6	r_w	0.09225	m
	m_w	2.5409	kg
	I_w	0.0083	kgm^2
8	r_w	0.123	m
	m_w	4.2253	kg
	I_w	0.0264	kgm^2

during assembly, and completely prevent reassembly of the prototypes. This is considered undesirable in an early design stage.

Design simplicity has been further ensured by keeping the number of part types low. The design is highly scalable, resulting in each prototype having exactly the same part types. All that is different are some dimensions.

The SFs of the critical components are within the specified range. For preliminary research, where users are able-bodied and know what to expect, and are being supervised, these safety factors are satisfactory. In the future, when supervision will be minimal and the user may not be very able, the users the SFs should be at least 4 to comply with the most strict guidelines. Further adding to the strictnes, NEN-EN-IEC 60601-1 specifies the reference mass should be 135kg, instead of the 80kg that is currently used. Increasing the SFs will inevitably lead to an even larger and heavier device. The first two future research topics might combat this.

Future research topics related to the prototype design:

- Slimming and trimming the wheels. Currently, the wheels are solid disks. A lot of material could be saved by making them more spoke-like. This would require a thorough strength analysis though, to still ensure safety.
- Replacing the chain with a drive belt. A chain was initially used to highlight how the device could be fabricated out of bicycle parts. However, the chain can be quite noisy, especially when sliding against the flanges. A drive belt might do better in these aspects. Also, a belt is thinner than chain, allowing a slightly smaller sprocket radius. A belt may be inferior to a chain when it comes to accommodating lateral sway of the user, though this would depend on the width of the belt.
- Changing the O-ring material NBR proved to be a suboptimal choice for the wheels. It degrades within a matter of weeks due to UV light. EPDM rubber will last longer, at the expense of lower hardness (Shore A 70 instead of 90).

4

Evaluation

4.1. Introduction

In section 2.2 a combined model of the device and the SLIP model was used to predict the human interaction. The SLIP model has been tried and tested to explain the basic gait dynamics [24]. It is yet unknown if the model of the device is also true to reality. This chapter will validate the open-loop behavior of the model of the device.

Discrepancies will inevitably be present due to the friction that is not modeled. There will be a fairly constant friction between the sprocket and the wheel, and a more varying friction between the rails and the wheels and flanges.

4.2. Methods: Motion-capture Experiments

Using a series of experiments, the model will be compared with the realized device. Different input trajectories will be applied to the end-effector by hand. Using motion-capture equipment, the trajectory and the resulting pulley trajectory will be recorded. Using a PD controller ($K_\mathrm{p} = 10^6\mathrm{Nm}^{-1}$ and $K_\mathrm{d} = 10^4\mathrm{Nsm}^{-1}$) the recorded trajectory will then be fed to the end-effector of the model. The horizontal pulley position will be compared for the model and the prototype. The position of the pulley relative to the end-effector determines the force that is exerted on the end-effector, so instead of measuring the force, these experiments measure the pulley position as output metric.

Two different experiments will be used. In the experiment 1, the end-effector will be moved in a vertical line. The upwards motion will make the pulley roll forward, the downwards motion will make the pulley roll back. In experiment 2 an arbitrary trajectory will be applied to the end-effector. Both experiments will be performed with each pulley size (R=2,4,6,8). Experiment 1 consists of 1 continuous measurement for each R, experiment 2 consists of 4 separate trials for each R.

Figure 4.1 shows the experimental setup. Markers are placed on the center axis of the pulley (both ends), start and end of the rail (both sides) and on the end-effector (front, back, left and right side). Figure 4.2 summarises the two different experiments.

The resolution of the Qualisys motion capture system was 0.7044 mm, the sampling frequency was 300 frames per second. The Kistler 9260AA6 force plates had a sensitivity setting of 19.008 mV/N in the vertical direction and 39.745 mV/N in horizontal directions, and a sampling frequency of 3000 frames per second.

The force plate data turned out to be too noisy to use, hence the pulley location is used as output metric. The noise is likely caused by the stacked table construction which supports the force plates. Additional details are included in Appendix B.

4.3. Results: Response to Input Trajectory

Figure 4.3 shows the results of both experiments.

Table 4.1 shows the root-mean-square (RMS) error between the simulated and motion-capture measured pulley position. It also shows the RMS error between the position of the end-effector that is measured by the motion capture system and the position of the end-effector in the simulation.

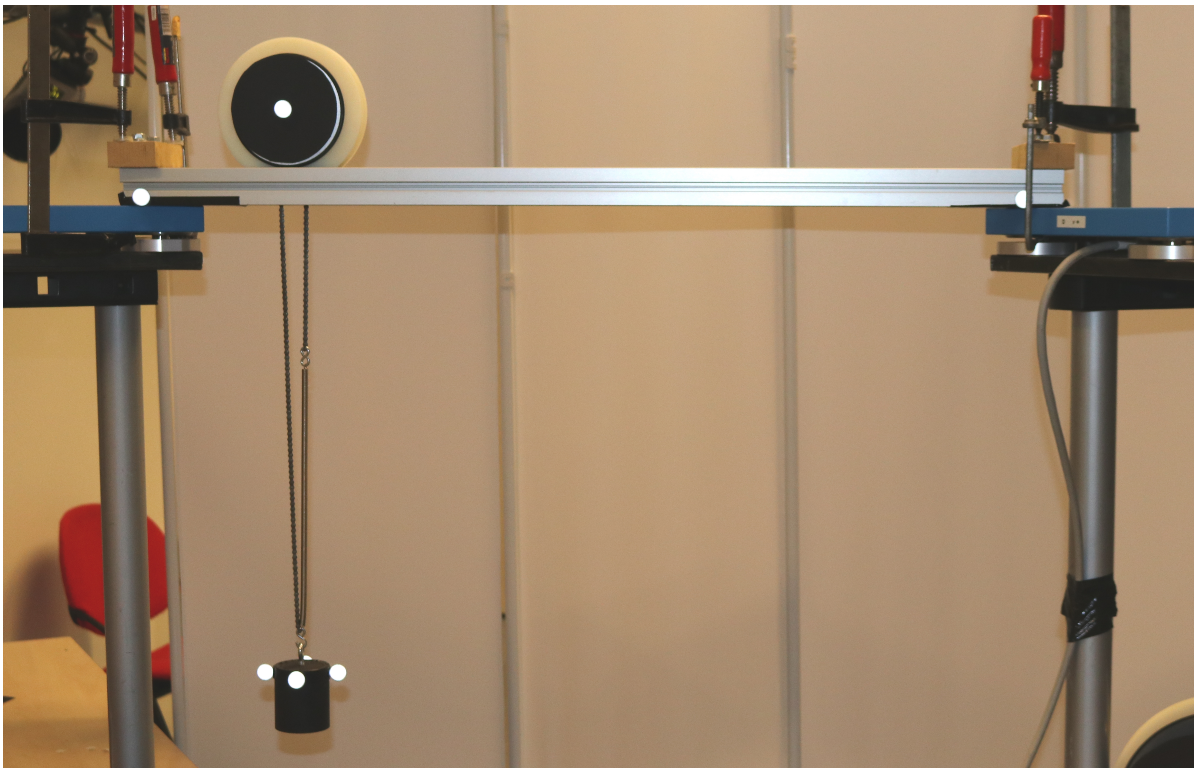

Figure 4.1: Picture of the experimental setup. The rail (silver) is secured to the force plates (blue) using clamps (handles in red). The force plates are placed on a table to generate sufficient space for the end-effector under the rail. The pulley is placed on the rail and the end-effector suspended from the pulley.

4.4. Discussion

Experiment 1 is sensitive to positional misalignments. In figures 4.3a through 4.3g, in the first few seconds, the motion capture system records no pulley movement, yet the simulation produces some movement. This is caused by the end-effector not being exactly below the pulley. This results in a horizontal force on the pulley. This force is small, and in reality friction will prevent the pulley from moving, though in a frictionless simulation the pulley will move. In future experiments it may prove wise to control the end-effector position more accurately.

The results in experiment 1 are inaccurate, and get more inaccurate as R increases. The RMS errors range from 15% to 130% of the total pulley displacement. There are a number of reasons for the inaccuracies:

- The way in which slackness is modelled.
  In Chapter 2 the slackness in the chain that connects the end-effector and sprocket was model using a unilateral controller, and the slackness in the chain that connects the spring and the sprocket was not modeled. It was then assumed that the end-effector would always be loaded and thus the spring would always be in tension. During the experiments, when moving too far up, the spring lost tension, leading

Table 4.1: RMS error value between the simulated and measured pulley position, as well as between the desired and the actual end-effector trajectory of the simulation.

	Experiment 1		Experiment 2	
R	Experiment RMS (m)	Controller RMS (mm)	Experiment RMS (m)	Controller RMS (mm)
2	0.0177	0.0577	0.0179	0.0626
4	0.0370	0.0540	0.0205	0.0578
6	0.0596	0.0597	0.0325	0.0634
8	0.0787	0.0619	0.0865	0.1010

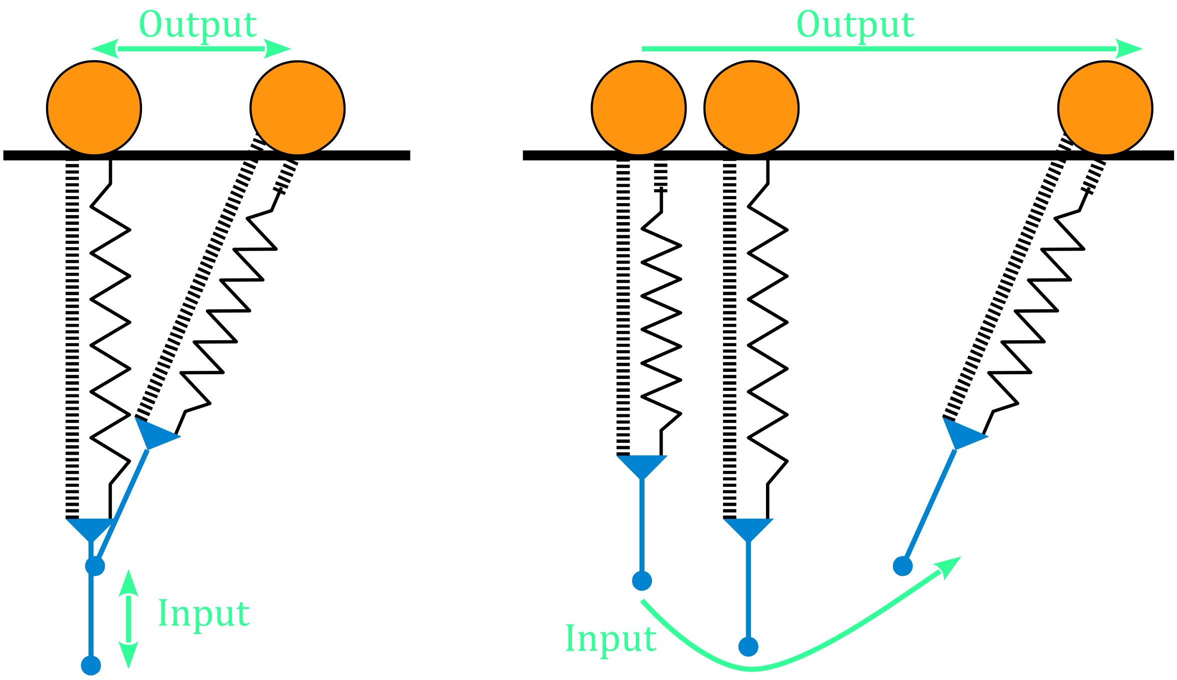

Figure 4.2: Schematic overview of the two experiments, including input and output measurements. Left (experiment 1): The end-effector of the device is moved up-and-down, and as a result the pulley will move back-and-forth. Right (experiment 2): An arbitrary trajectory will be applied to the end-effector and the pulley can respond by either following the end-effector or moving ahead of it.

to erratic behavior of the simulation.

It can be observed, for example in Figure 4.3e, peaks 2 through 6, that the pulley stops moving forward because it reaches the maximum angle imposed by R. The simulation, lacking the slackness condition, continues moving the pulley forward as long as the end-effector keeps moving forward. The effect can also be observed in Figure 4.3e, all peaks, and in Figure 4.3g, peak 1. Figure 4.3a does not suffer from this problem, for the device does not reach the maximum angle imposed by R.

- Relatively low spring stiffness
  The spring used during the experiments is relatively weak. This was done to ensure being able to move it by hand. In the actual use case the springs will be much stiffer. The inertia, however, was equal to the actual use case of the device. In Figure 4.3a this leads to the baseline elevation of the motion-capture data. When reaching that maximum horizontal displacement that the height of the end-effector imposes, the pulley rolls on a tiny bit more. The sprocket has come to a stop because the end-effector has, but the wheels roll on a little more. When the wheels want to roll back again the ratchet engages and the sprocket also has to roll back.

  The relatively high inertia also leads to some overshoots when the device settles at a certain position. In figure 4.3e four and a half real peaks can be observed in the motion-capture data. In the first and third peak the pulley overshoots the settling position a bit, before returning to the settling position. In Figure 4.3c, peak 3, 4 and 5 this can also be observed.

In experiment 2, for R=2,4,6 slightly lower RMS errors can be observed. The spring never goes slack in experiment 2, eliminating a source of error compared to experiment 1.

What makes experiment 2 different from experiment 1 is the horizontal movement of the end-effector. Horizontal movement of the end-effector causes the the pulley to move through kinetic means: the spring angle changes in response to end-effector displacement and the spring exerts a horizontal force component on the pulley. The pulley movement in experiment 1 was of a more kinematic nature. The vertical end-effector displacement and the horizontal pulley displacement are kinematically coupled by R and l. The friction will have a more detrimental effect in the kinetically induced movement. For example, in the motion capture plots of figure 4.3b, at t=3s and t≈8.3s a plateau can be observed. Friction momentarily stops the pulley from moving.

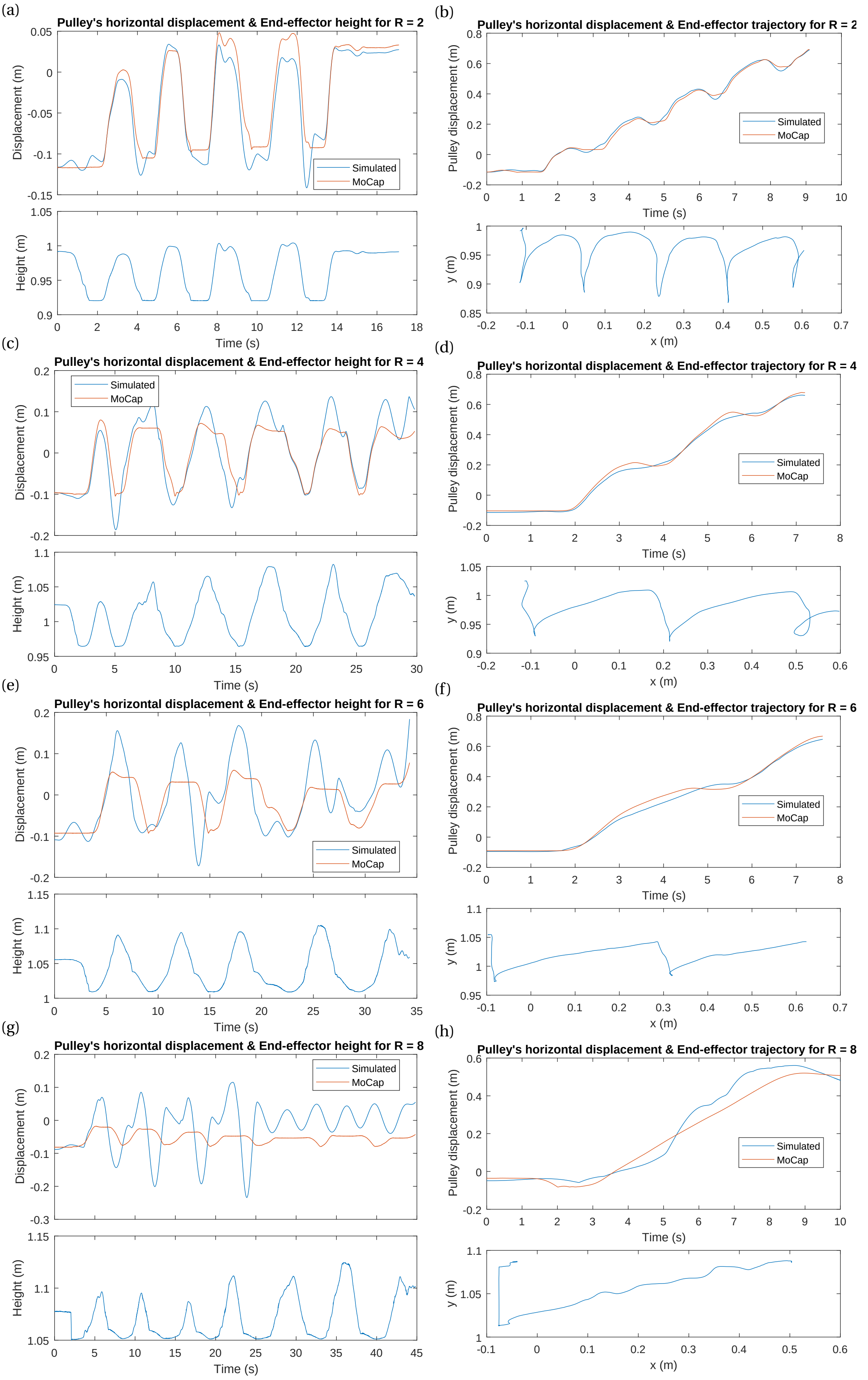

Figure 4.3: Plots showing results of the experiments. Subfigures a, c, e and g show the results of the vertical end-effector translation. Bottom graphs show the end-effector height which serves a input to the experiment, while the top graphs show the resulting pulley position output. Subfigures b, d, f and h show the results of the arbitrary end-effector trajectory. Bottom graphs show the trajectory of the end-effector, top graphs show the resulting pulley position.

An additional source of error could be the model properties. Maybe the dimension of the wheels are slightly larger, or maybe the stiffness of the rubber O-rings causes them to indent a little bit under load, resulting in a lower effective wheel radius. This might explain a tiny bit of the RMS error.

Evaluation might have been better with a separate device to apply the input trajectory, instead of doing it by hand. Compared to the development time and cost of this device, such an input device would be highly expensive and therefore it was not used. The future development will most likely be the more elongated version of the patent. This version fits in a conventional ceiling rail and it would be relatively easy to conduct experiments with humans in the loop, completely circumventing the need to for an input device.

The gains of the trajectory-enforcing controller could be higher to increase the fidelity of the controller, though this would have made the system of differential and algebraic equations even more stiff, significantly increasing the simulation times. Seeing how the RMS error of the controller is already a factor 1000 smaller in both experiments, increasing the controller gains is not a priority.

5

Discussion

5.1. Evaluation

The evaluation proved that the device can provide a forward force in response to an upwards motion of the end-effector. The quantitative predictions from the model of the device did not exactly match the results from the experiments, though. One part of the RMS error between the simulation and the experiments may be explained by the fact that sliding friction was not modeled. In the vertical oscillation experiment the initial end-effector position may not have been exactly below the pulley. This means the unloading force acts at an angle and there is a horizontal component acting on the pulley. In reality, when the angle is small, the pulley will not move because of the static friction between the flanges and the rail. In the model, however, the pulley will start moving. A second part of the of the discrepancies may be explained by the experimental protocol. Sometimes the end-effector went too far up, causing not only the chain, but also the spring to become slack. Slackness of the chain is modeled, slackness of the spring is not. In reality, the pulley will stop moving when the spring goes slack, however, the model does not, resulting in large RMS errors. Including a slack spring state in the model is not desirable. In the final application, the device will constantly unload body weight; the spring will always be under tension. Including the slack spring state in the model would only cater to a highly specific situation, which could be avoided by taking care the end-effector does not move up too far.

5.2. Mechanical Concept Realization

The single-axle embodiment could effectively be ported from concept to prototype. The main critique is that the weight of the wheels could be reduced. The strength of the ratchet currently limits the safety of the device and dimensions at large R are pushing the limits of practicality. The elongated embodiment could solve this. It may have lower inertia, and the inertia and dimensions would hardly scale with R. Additionally, it may employ side wheels instead of flanges to stay in the rail, reducing friction. Finally, the elongated embodiment can fit in a conventional ceiling rails. Being able to fit in existing and already-installed ceiling rails may be a huge benefit for successful reception of the device with clinicians.

5.3. Theoretical Concept Realization

Reduction of the deteriorating effects of BWU on the gait parameters could be observed, though it is limited to highly specific combinations of BWU and R, and also limited to the average velocity. The device can increase or decrease the average speed, based on R and BWU. The device can reduce the average height difference and increase the average step size.

The model did not contain friction, nor did it contain the user's neurological control. The effects of the user's neurological control can be investigated in human trials. Friction can be investigated by including friction in the model of the device, and then coupling that model with a nonconservative model of human gait.

In a regular trolley or in the inactive device, friction between the device and the rail is felt as a horizontal force on the user. When the device activates, there is a kinematic coupling between the upwards motion of the end-effector and the horizontal motion of the pulley of the device. Dynamic friction experienced by the pulley is now experienced as friction on moving upwards for the user. This means friction will be felt as a reduction of the vertical unloading force. This is potentially advantageous because a relatively small change in an already existing force is potentially less impactful for gait control than a new force appearing out of nowhere.

5.4. Introduction

The analyzed device is capable of providing a forward force, based on the trajectory of the user. In simulations the device generally did not reduce the gait deteriorations that occurred due to BWU. Maybe a forward force is not the answer to the gait deteriorations of BWU, or maybe the forward force needs to be configured differently. Currently, the forward force gradually grows to its maximum as the user moves up. At the starts of moving up, during the toe-off power event, the device provides little forward force. Thus, the device hardly aids the toe-off power event, which is the main power event during gait [9]. Instead, the device mainly aids the hip extension power event. There is no reason why the hip extension would need more assistance than the toe-off event. Future research may investigate how to distribute the assistance equally over the power events that occur during gait.

Alternatively, a net forward force may not be required. Instead, the forward force of the device may serve to compensate the friction forces that the user experiences as a backwards force.

6

Conclusion

6.1. Summary

In Chapter 1 it was hypothesized how and why a forward force may have a positive effect gait rehabilitation. A novel patent was introduced which can passively provide a forward force. The concept, its basic functionality and the limitations were detailed. Chapter 2 elaborated on the concept with a static analysis. This static analysis provided some insights about the functionality and limitations of the device, and showed that parameter with the greatest influence on the angle of the unloading force was R. In a simulation, the device was coupled to the SLIP model, to make predictions about the human interaction of the device. This showed that the device generally deteriorated the parameters of unloaded gait. Only for the average velocity a small improvement could be observed. Chapter 3 details the construction of multiple prototypes, which were used in Chapter 4 to compare the model of the device against the realized device. Qualitatively the experiments matched the model predictions, but quantitatively there were notable differences. The discrepancies could be partially accounted for.

6.2. Future Work

The following topics could provide interesting follow-up research, to expand on, or to improve parts of this thesis, in no particular order:

- Redo the evaluation
  A large part of the RMS errors in the experiments are caused by the spring going slack and the friction causing the end-effector not returning to exactly above the end-effector. Redoing the evaluation while preventing the spring from going slack and ensuring the end-effector moves strictly horizontal is expected to reduce a large portion of the current RMS errors.

- Human trials
  The model of the device does not include friction and the SLIP model does not allow for adjustments of neurological control of gait. Using a human trial those features could be investigated in great detail. This will also allow for more definite conclusions regarding the deterioration or amelioration of the gait parameters.

- Elongated prototype
  The elongated prototype features smaller dimensions and a smaller mass, and it also has more potential to meet the safety norm. The elongated prototype can also be combined with the human trials. Having a device that fits in a certified rail certainly pleases the ethics committee.

- Assist toe-off
  The current device mainly assists the hip extension power event. Additional research could look into how assistance may be distributed more equally over the hip extension and the toe-off power events.

A

Simulation

A.1. Equations of Motion

Figure A.1 shows the the model again. Using Euler-Lagrange the equations of motion will be derived.

Using the following set of generalized coordinates:

$$\boldsymbol{q} = \begin{pmatrix} \phi_{\mathrm{w}} \\ \phi_{\mathrm{s}} \\ x_{\mathrm{b}} \\ y_{\mathrm{b}} \end{pmatrix} \tag{A.1}$$

the kinetic and potential energy terms of the system's components can be expressed. The datum for potential energy is at the origin of the coordinate system. The x coordinates where the front and back foot touch the ground are denoted by the respective subscripts.

$$V_{\mathrm{w}} = mg(h + r_{\mathrm{w}}) \tag{A.2}$$

$$T_{\mathrm{w}} = \frac{1}{2}(m_{\mathrm{w}} r_{\mathrm{w}}^2 + I_{\mathrm{w}})\dot{\phi}_{\mathrm{w}}^2 \tag{A.3}$$

$$V_{\mathrm{s}} = mg(h + r_{\mathrm{w}}) \tag{A.4}$$

$$T_{\mathrm{s}} = \frac{1}{2} m_{\mathrm{s}} r_{\mathrm{w}}^2 \dot{\phi}_{\mathrm{w}}^2 + \frac{1}{2} I_{\mathrm{s}} \dot{\phi}_{\mathrm{s}}^2 \tag{A.5}$$

$$\Delta x = -r_{\mathrm{w}}\phi_{\mathrm{w}} - x_{\mathrm{b}} \tag{A.6}$$

$$\Delta y = h + r_{\mathrm{w}} - y_{\mathrm{b}} \tag{A.7}$$

$$\theta = \tan^{-1}\left(\frac{\Delta x}{\Delta y}\right) \tag{A.8}$$

$$l = \sqrt{\Delta x^2 + \Delta y^2} \tag{A.9}$$

$$V_{\mathrm{spring}} = \frac{1}{2} k(l + (\theta + \phi_{\mathrm{s}}) r_{\mathrm{s}} - L)^2 \tag{A.10}$$

$$T_{\mathrm{b}} = \frac{1}{2} m(x_{\mathrm{b}}^2 + y_{\mathrm{b}}^2) \tag{A.11}$$

$$V_{\mathrm{b}} = mg y_{\mathrm{b}} \tag{A.12}$$

$$V_{\mathrm{front}} = \frac{1}{2} k_{\mathrm{leg}}\left(\sqrt{(x_{\mathrm{front}} - x_{\mathrm{b}})^2 + y_{\mathrm{b}}^2} - L_0\right)^2 \tag{A.13}$$

$$V_{\mathrm{back}} = \frac{1}{2} k_{\mathrm{leg}}\left(\sqrt{(x_{\mathrm{b}} - x_{\mathrm{back}})^2 + y_{\mathrm{b}}^2} - L_0\right)^2 \tag{A.14}$$

$$\tag{A.15}$$

The various kinetic and potential terms are then summed up to find the total kinetic and potential energy in the system. There are two states, one where only the back leg touches the ground, and one where both the

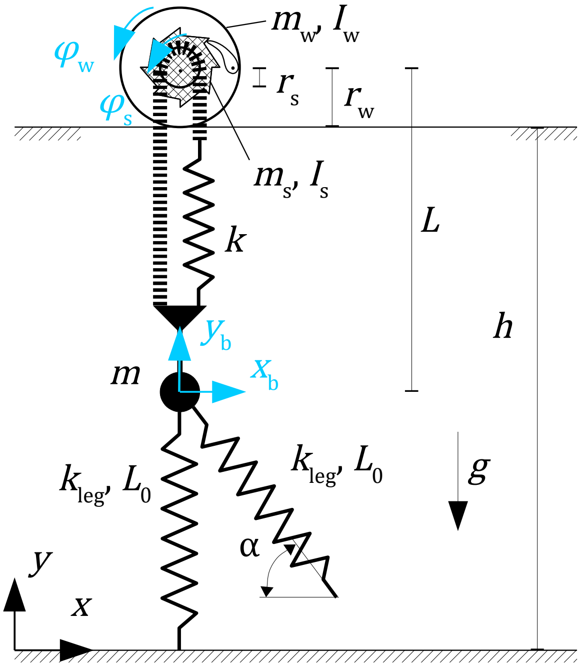

Figure A.1: Overview of the combined model of the device and the SLIP model.

back and the front leg touch the ground. In order to determine the equations of motion for either system, substitute either V_1 or V_2 for V.

$$T = T_w + T_s + T_b \tag{A.16}$$

$$V_1 = V_w + V_s + V_b + V_{spring} + V_{back} \tag{A.17}$$

$$V_2 = V_w + V_s + V_b + V_{spring} + V_{back} + V_{front} \tag{A.18}$$

$$\tag{A.19}$$

Euler-lagrange now formulates the equations of motion as follows:

$$\frac{\mathrm{d}}{\mathrm{d}t}\left(\frac{\partial T}{\partial \dot{\boldsymbol{q}}}\right) + \frac{\partial V}{\partial \boldsymbol{q}} = \boldsymbol{Q} \tag{A.20}$$

Where $\boldsymbol{Q}$ denotes the generalized forces that are applied. For numerical integration it is preferred to have the equations of motion in the form:

$$\mathbf{M}\ddot{\boldsymbol{q}} = \boldsymbol{f} \tag{A.21}$$

This form also allows for expansion of the equations of motion with constraints later on. Expanding and rearranging equation A.20 yields:

$$\frac{\partial}{\partial \dot{\boldsymbol{q}}}\left(\frac{\partial T}{\partial \dot{\boldsymbol{q}}}\right)\ddot{\boldsymbol{q}} = -\frac{\partial}{\partial \boldsymbol{q}}\left(\frac{\partial T}{\partial \dot{\boldsymbol{q}}}\right)\dot{\boldsymbol{q}} + \frac{\partial T}{\partial \boldsymbol{q}} - \frac{\partial V}{\partial \boldsymbol{q}} + \boldsymbol{Q} \tag{A.22}$$

Where

$$\mathbf{M} = \frac{\partial}{\partial \dot{\boldsymbol{q}}}\left(\frac{\partial T}{\partial \dot{\boldsymbol{q}}}\right) \tag{A.23}$$

$$f = -\frac{\partial}{\partial \boldsymbol{q}}\left(\frac{\partial T}{\partial \dot{\boldsymbol{q}}}\right)\dot{\boldsymbol{q}} + \frac{\partial T}{\partial \boldsymbol{q}} - \frac{\partial V}{\partial \boldsymbol{q}} + \boldsymbol{Q} \tag{A.24}$$

In equation A.24 either V_1 or V_2 can be substituted to find the equations of motion of the system with 1 respectively 2 legs touching the ground.

The system starts with 1 leg touching the ground, as depicted in Figure A.1. When the front leg, held at angle α touches the ground, it connects to the ground. The distance between the ground the foot is given by $\delta_1 = y_b - L_0 \sin\alpha$. Matlab's event detection can detect negative-direction zero crossings of δ_1. When it does, integration of the single-stance EoM will stop and integration of the double-stance EoM will commence from the ending state.

When the back leg is no longer compressed, it detaches from the ground. The compression of the spring is given by: $\delta_2 = L_0 - \sqrt{(x_\text{b} - x_\text{back})^2 + y_\text{b}^2}$. Matlab's event detection can detect negative-direction zero crossings of δ_2. When it does, integration of the souble-stance EoM will stop. The old front leg becomes the new back leg and integration of the single-stance EoM will commence from the ending state.

A.2. Ratchet Constraint

The ratchet occasionally provides a constraint on the system. When $\phi_\text{s} \geq \phi_\text{w}$ the ratchet freely permits motion. When $\phi_\text{s} < \phi_\text{w}$ the ratchet provides a torque to ensure $\phi_\text{s} = \phi_\text{w}$. When the ratchet exerts a torque, the constraint function is:

$$\Phi(\dot{\boldsymbol{q}}) = \dot{\phi}_w - \dot{\phi}_s = 0 \tag{A.25}$$

This function is not integrable (the integration constant would be different each time the ratchet engages), making it a nonholonomic constraint. In order to include this constraint in the equations of motion, the constraint needs to be linear in the accelerations and a Lagrange multiplier $\boldsymbol{\tau}$ needs to be defined.

$$\frac{\partial \Phi}{\partial \dot{\boldsymbol{q}}} \ddot{\boldsymbol{q}} = \mathbf{0} \tag{A.26}$$

Doing so yields the expanded equation of motion:

$$\begin{bmatrix} \mathbf{M} & \left(\frac{\partial \Phi}{\partial \dot{\boldsymbol{q}}}\right)^T \\ \frac{\partial \Phi}{\partial \dot{\boldsymbol{q}}} & \mathbf{0} \end{bmatrix} \begin{pmatrix} \ddot{\boldsymbol{q}} \\ \boldsymbol{\tau} \end{pmatrix} = \begin{pmatrix} \boldsymbol{f} \\ \mathbf{0} \end{pmatrix} \tag{A.27}$$

The equations of motion use the acceleration constraint, whereas the original constraint was in velocity space. Due to drift (numerical integration errors caused by the fact that the order of the approximation is finite) the results may be inaccurate. One solution to this is coordinate projection. Projecting your coordinates back to the constraint space after every integration step. While this method is optimal in terms of improving the accuracy of the solution with respect to the constraints, it can not be combined with Matlab's ode solver's and Matlab's event detection. An alternative method is to use state-space stabilization methods such as Baumgarte's method [30]. Baumgarte suggested to implement negative feedback on the constraint errors. The velocity constraint errors are multiplied by the error gain γ and fed back to the acceleration constraint function.

$$\frac{\partial \Phi}{\partial \dot{\boldsymbol{q}}} \ddot{\boldsymbol{q}} = \mathbf{0} \rightarrow \frac{\partial \Phi}{\partial \dot{\boldsymbol{q}}} \ddot{\boldsymbol{q}} = \mathbf{0} - \gamma \Phi(\dot{\boldsymbol{q}}) \tag{A.28}$$

This will not completely get rid of the constraint error, but it does reduce them and prevents them from growing continously as is the case with drift. The gain was experimentally tuned to $\gamma = 1000\text{s}^{-1}$. The new expanded equations of motion now look like this:

$$\begin{bmatrix} \mathbf{M} & \left(\frac{\partial \Phi}{\partial \dot{\boldsymbol{q}}}\right)^T \\ \frac{\partial \Phi}{\partial \dot{\boldsymbol{q}}} & \mathbf{0} \end{bmatrix} \begin{pmatrix} \ddot{\boldsymbol{q}} \\ \boldsymbol{\tau} \end{pmatrix} = \begin{pmatrix} \boldsymbol{f} \\ -\gamma \Phi(\dot{\boldsymbol{q}}) \end{pmatrix} \tag{A.29}$$

Equations A.21 and A.29, with the appropriate substitution for V, provide the equations of motion of the model of the device. Numerical integration starts with the unexpanded EoM. When the event detector detects a positive-direction zero crossing of $\Phi(\dot{\boldsymbol{q}})$ integration stops and integration of the expanded equations of motion commences from the ending state. When the event detector detects a negative-direction zero crossing of $\boldsymbol{\tau}$ integration of the expanded equations of motion stops, and integration of the unexpanded equations of motion commences from the ending state.

A.3. Slack Chain Constraint

The final constraint that needs to be included is the chain that connects the sprocket and end-effector. This chain can be slack or taut. When it is slack it does not exert a force on the sprocket and end-effector, when it is taut it does. This constraint is implemented using a switching controller. When the chain is slack it does not act, when the chain is taut it behaves as a stiff (relative to the rest of the system) PD controller.

The error function is governed by the rest length of the chain L_0 (length from center of sprocket to end-effector) and the relative rotation of the chain around the sprocket, $(\theta+\phi_\mathrm{s})r_\mathrm{s}$. This is compared to the actual distance between the end-effector and the center of the sprocket.

$$\Delta x = -r_\mathrm{w}\phi_\mathrm{w} - x_\mathrm{b} \tag{A.30}$$

$$\Delta y = h + r_\mathrm{w} - y_\mathrm{b} \tag{A.31}$$

$$\theta = \tan^{-1}(\frac{\Delta x}{\Delta y}) \tag{A.32}$$

$$l = \sqrt{\Delta x^2 + \Delta y^2} \tag{A.33}$$

$$\epsilon = l - (L_0 + (\theta+\phi_\mathrm{s})r_\mathrm{s}) \tag{A.34}$$

$$\dot{\epsilon} = \frac{\partial \epsilon}{\partial \boldsymbol{q}}\dot{\boldsymbol{q}} \tag{A.35}$$

Using gains K_p and K_d this error can be converted to a force.

$$F = K_p \max(\epsilon, 0) + K_p\dot{\epsilon}\ \underbrace{\max(\min(\epsilon,1),0)}_{\text{Improvised step function}} \tag{A.36}$$

Where $K_\mathrm{p} = 10^6\mathrm{Nm}^{-1}$ and $K_\mathrm{d} = 10^8\mathrm{Nsm}^{-1}$. In order to be able to implement them using Matlab's Symbolic Toolbox, the min and max functions were implemented slightly differently:

$$\max(a,b) \quad \Leftrightarrow \quad a + b + \mathrm{abs}(a-b) \tag{A.37}$$

$$\min(a,b) \quad \Leftrightarrow \quad a + b - \mathrm{abs}(a-b) \tag{A.38}$$

Next, the force needs to be included in the equations of motion. The controller force is translated from Cartesian to generalized coordinates and then included in $\boldsymbol{Q}$.

$$\boldsymbol{Q} = \frac{\partial \boldsymbol{x}}{\partial \boldsymbol{q}}\boldsymbol{F} \tag{A.39}$$

Where x_vec is the vector containing the Cartesian coordinates of the bodies. In order: x coordinate, y coordinate and angle of the wheel, x coordinate, y coordinate and angle of the sprocket and finally the x and y coordinate of the body.

$$\boldsymbol{x} = \begin{pmatrix} -r_\mathrm{w}\phi_\mathrm{w} \\ 0 \\ \phi_\mathrm{w} \\ -r_\mathrm{w}\phi_\mathrm{w} \\ 0 \\ \phi_\mathrm{s} \\ x \\ y \end{pmatrix} \tag{A.40}$$

and $\boldsymbol{F}$ is the vector that translates how F acts on each body:

$$\boldsymbol{F} = \begin{pmatrix} 0 \\ 0 \\ 0 \\ -F\sin(\theta) \\ -F\cos(\theta) \\ Fr_\mathrm{s} \\ F\sin(\theta) \\ F\cos(\theta) \end{pmatrix} \tag{A.41}$$

A.4. Numerical Integration

Four different sets of equations of motion have been determined; single stance or double stance, and ratchet engaged or disengaged. Numerical integration was performed using Matlab's `ode15s` solver, switching between sets of equations of motion as appropriate Switching occurred one state at a time. Either the amount of stance legs or the engagement of the ratchet changed, never both at the same time. Should both events have been triggered, the changes will occur sequentially, but the stance leg switch will take precedence. Both switches will occur at the same point in (simulation) time though.

A relative tolerance of 10^{-7} and absolute tolerance of 10^{-9} were used. Aside from the events mentioned, integration also stopped when the simulation time exceeds 10s.

B

Force Plate Data

The rail is supported by two force plates. The force plates are both supported by two stacked tables. The tables are extremely stiff in the vertical direction but relatively compliant in the directions orthogonal to the vertical direction.

Figure B.1 shows the force plate data of the vertical oscillation experiment, with $R = 2$. The vertical force data has a very low noise-to-data ratio. The forward and lateral force data have a much higher noise-to-data ratio.

This is likely caused by the relatively compliant support structure. The support structure has a multitude of eigenmodes which may be excited during the experiment. The force plates will mainly be recording the eigenmodes and stiffness of the support structure rather than the data of interest, which is the force that the pulley exerts on the rails. For this reason the force plate data is omitted and the pulley location is used instead as an output metric of the experiment.

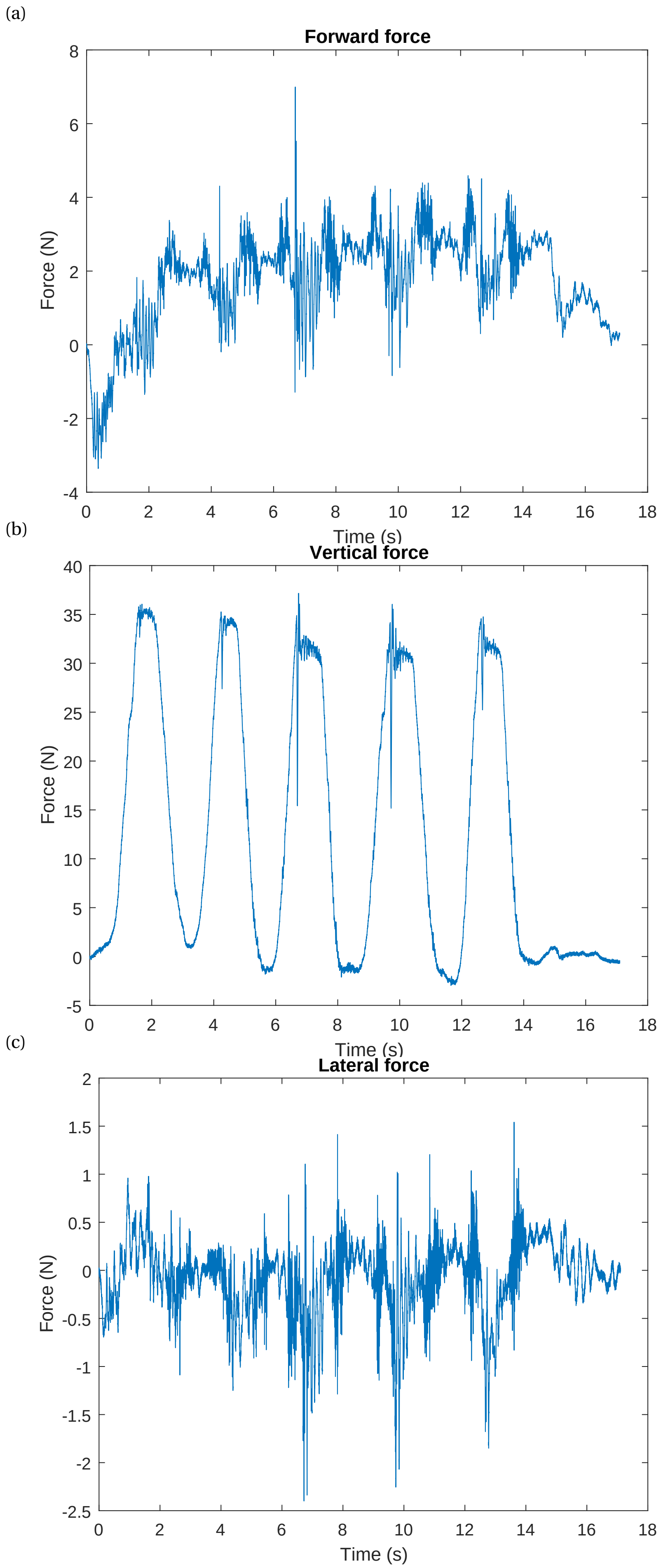

Figure B.1: Force data of one of the force plates during the vertical oscillation experiment for $R = 2$.

C

Technical Drawings

Please note that the drawings are slightly compressed due to LaTeX, and therefore they are not to scale.

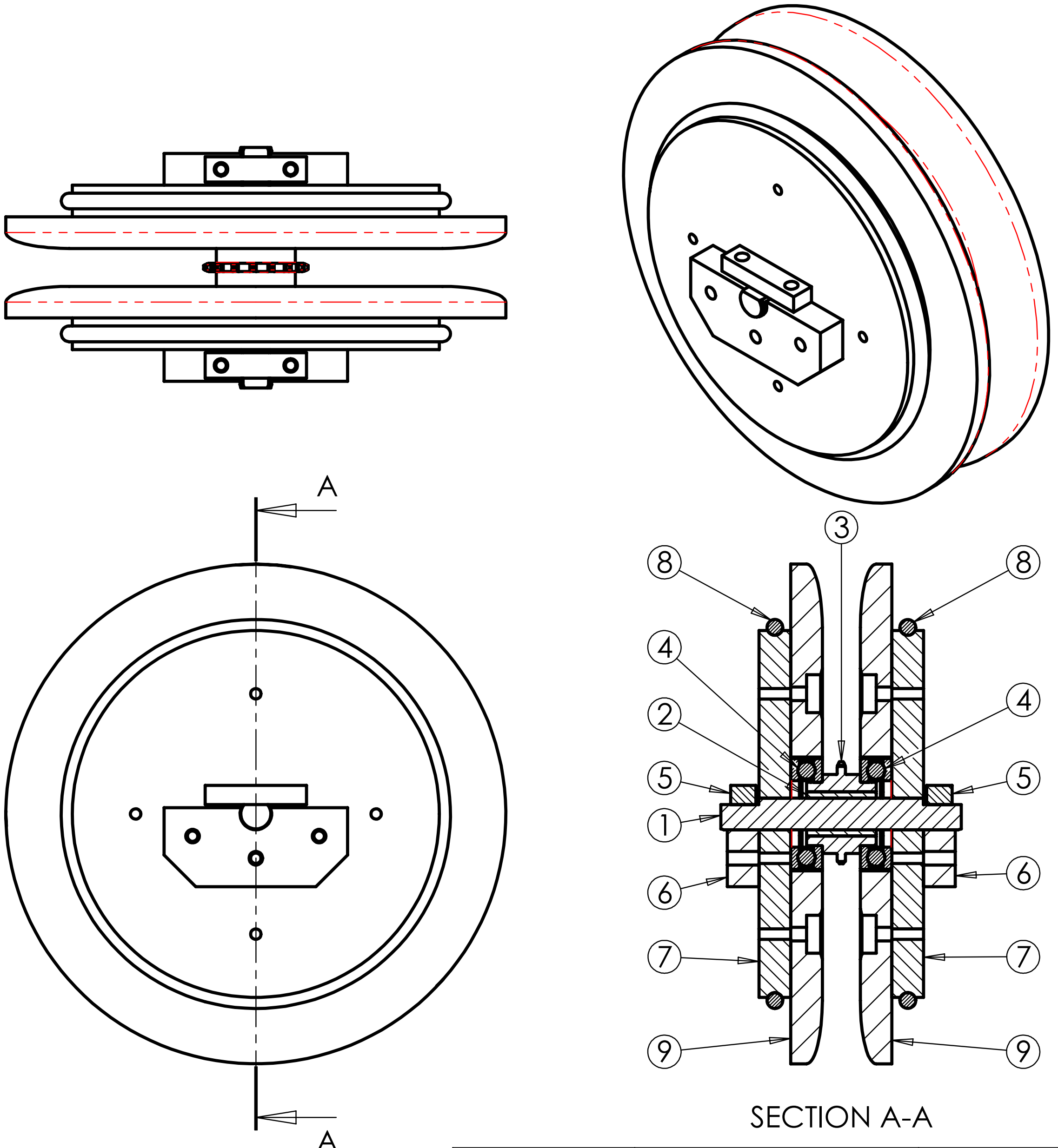

ITEM NO	PART NAME	QTY
1	Shaft	1
2	Freewheel	1
3	Sprocket	1
4	Axial bearing	2
5	Connector	2
6	Hub	2
7	Wheel	2
8	O-ring	2
9	Flange	2

ROUGHNESS:	MATERIAL:	FINISH:	MASS [g]:	GEN.TOL.:	QTY.: 4	REV.:

THIRD ANGLE PROJECTION

SCALE: 1:2
DIMENSIONS: mm
DATE: 14-2-2018

DRAWN BY: JBJvdS
DESGN. BY:
PROJECT:

Drawing No:

Delft Biorobotics Laboratory
Mekelweg 2, 2628 CD Delft
P +31 (0)15 2785614

DESCRIPTION:

Assembly

A4

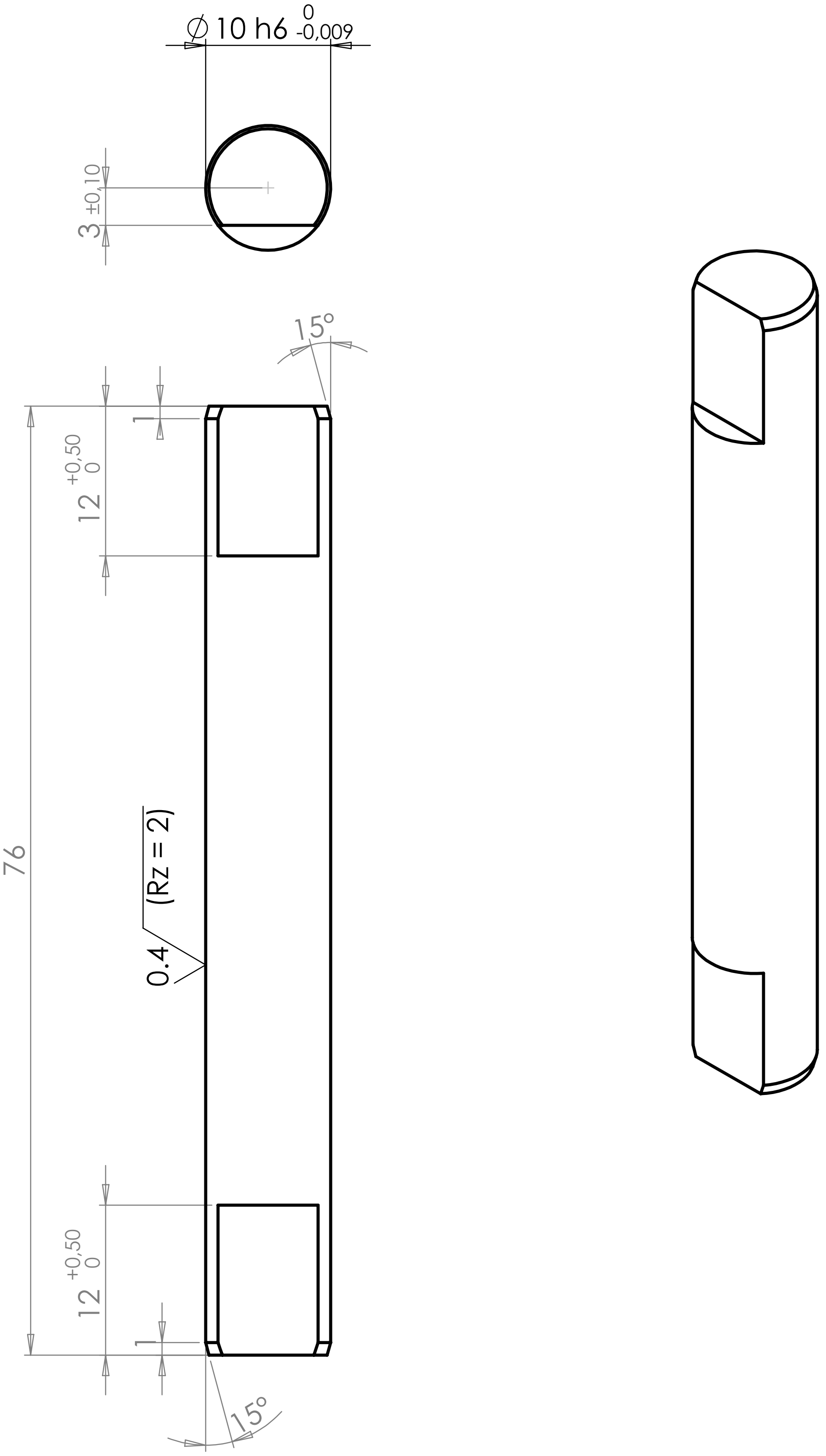
∅ 10 h6 0 -0,009
3 ±0,10
15°
1
12 +0,50 0
76
0.4 (Rz = 2)
12 +0,50 0
1
15°

ROUGHNESS: 3.2	MATERIAL: Case-hardened steel	FINISH:	MASS [g]:	GEN.TOL.: ±0.2	QTY.: 4	REV.:
THIRD ANGLE PROJECTION	SCALE: 2:1	DRAWN BY: JBJvdS		Drawing No:		
	DIMENSIONS: mm	DESGN. BY:				
	DATE: 12-2-2018	PROJECT:				
Delft Biorobotics Laboratory **Mekelweg 2, 2628 CD Delft** **P +31 (0)15 2785614**		DESCRIPTION: Shaft				A4

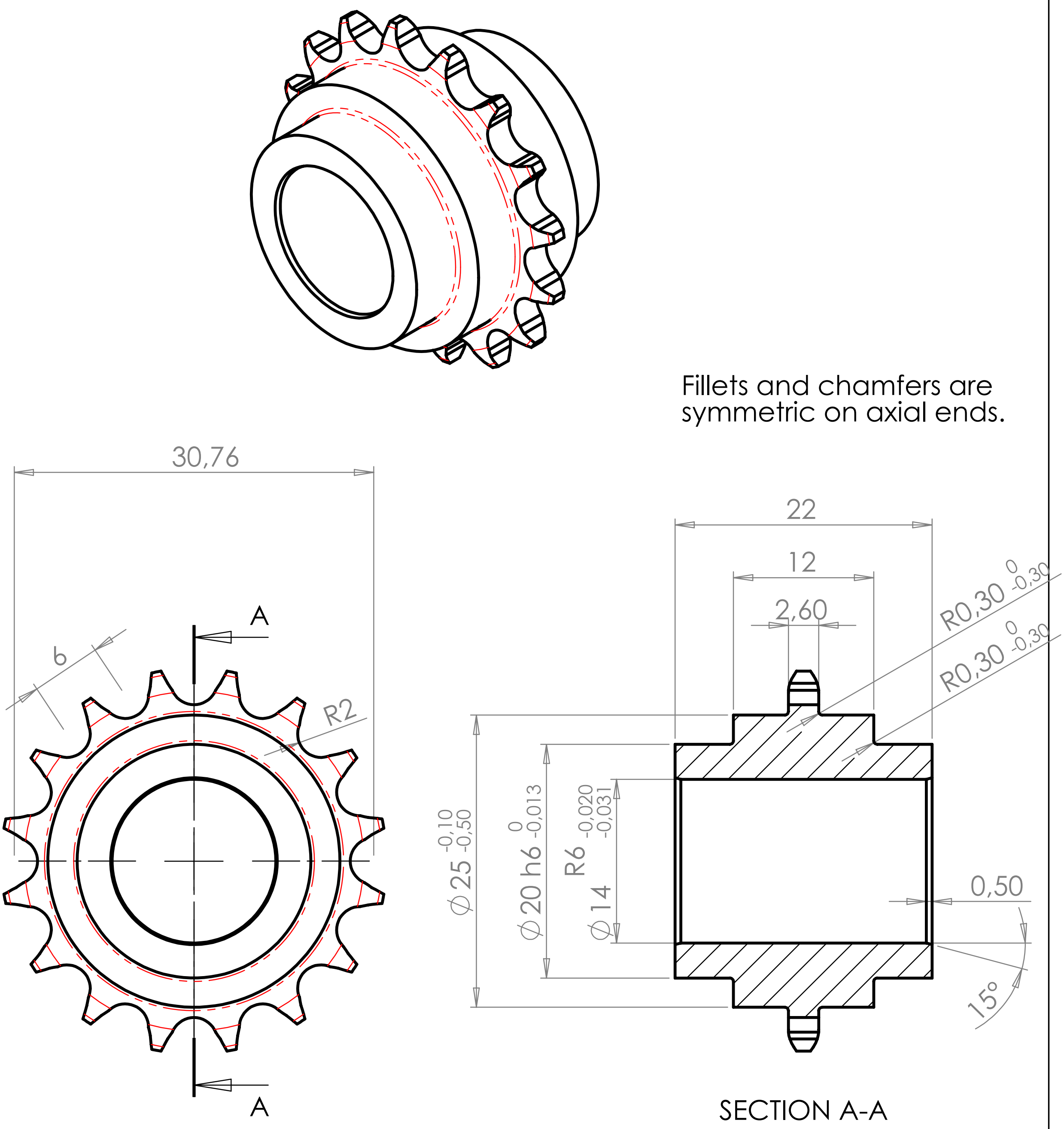
30,76
A
6
R2
A
22
12
2,60
R0,30 0 -0,30
R0,30 0 -0,30
Ø 25 -0,10 -0,50
Ø 20 h6 0 -0,013
R6 -0,020 -0,031
Ø 14
0,50
15°
SECTION A-A

Fillets and chamfers are symmetric on axial ends.

ROUGHNESS: 0.8	MATERIAL: Aluminium 7075	FINISH:	MASS [g]:	GEN.TOL.: ±0.1	QTY.: 4	REV.:
THIRD ANGLE PROJECTION	SCALE: 2:1	DRAWN BY: JBJvdS		Drawing No:		
	DIMENSIONS: mm	DESGN. BY:				
	DATE: 12-2-2018	PROJECT:				
TUDelft **Delft Biorobotics Laboratory** **Mekelweg 2, 2628 CD Delft** **P +31 (0)15 2785614**		DESCRIPTION: Sprocket				A4

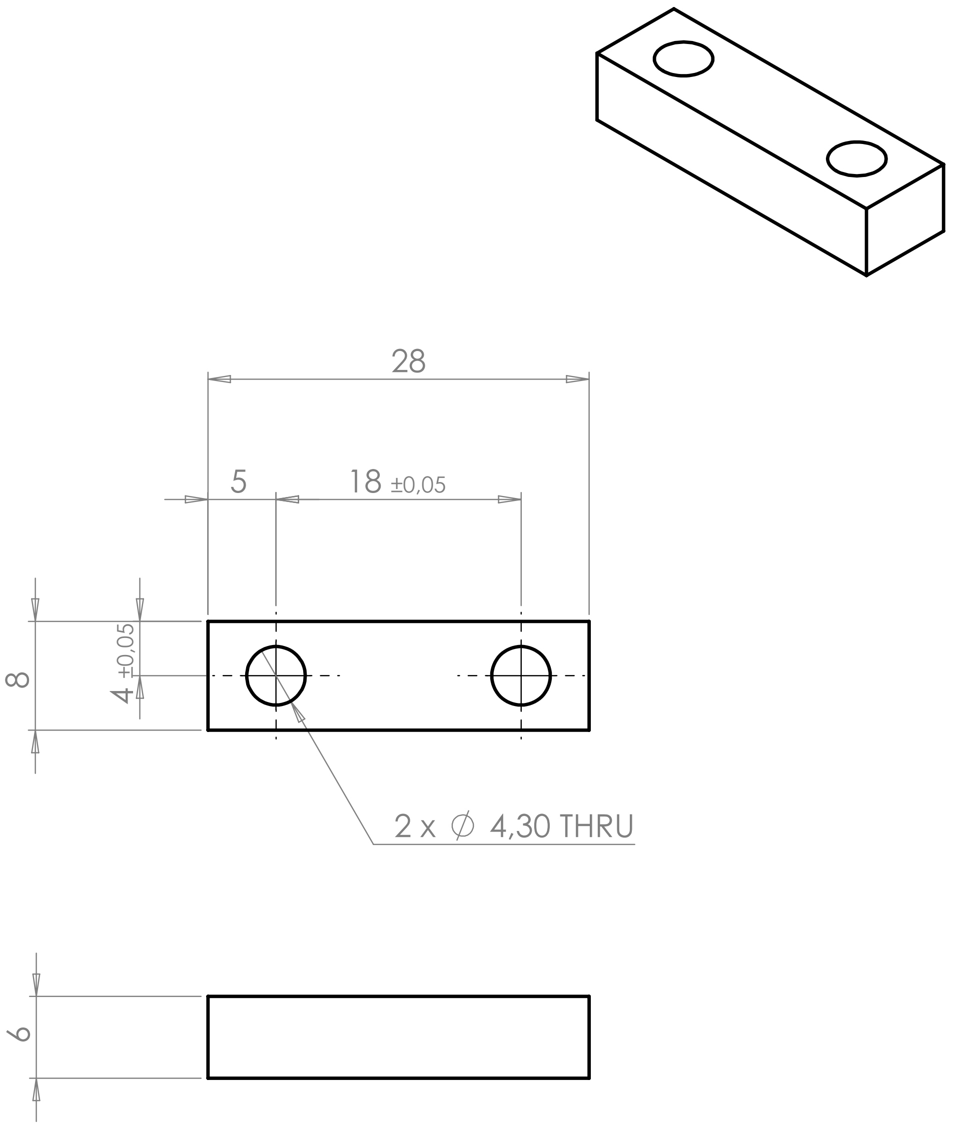

ROUGHNESS: 3.2	MATERIAL: Aluminium 7075	FINISH:	MASS [g]:	GEN.TOL.: ±0.1	QTY.: 2	REV.:
THIRD ANGLE PROJECTION	SCALE: 2:1	DRAWN BY: JBJvdS		Drawing No:		
	DIMENSIONS: mm	DESGN. BY:				
	DATE: 12-2-2018	PROJECT:				
TUDelft **Delft Biorobotics Laboratory** **Mekelweg 2, 2628 CD Delft** **P +31 (0)15 2785614**		DESCRIPTION: Connector2				A4

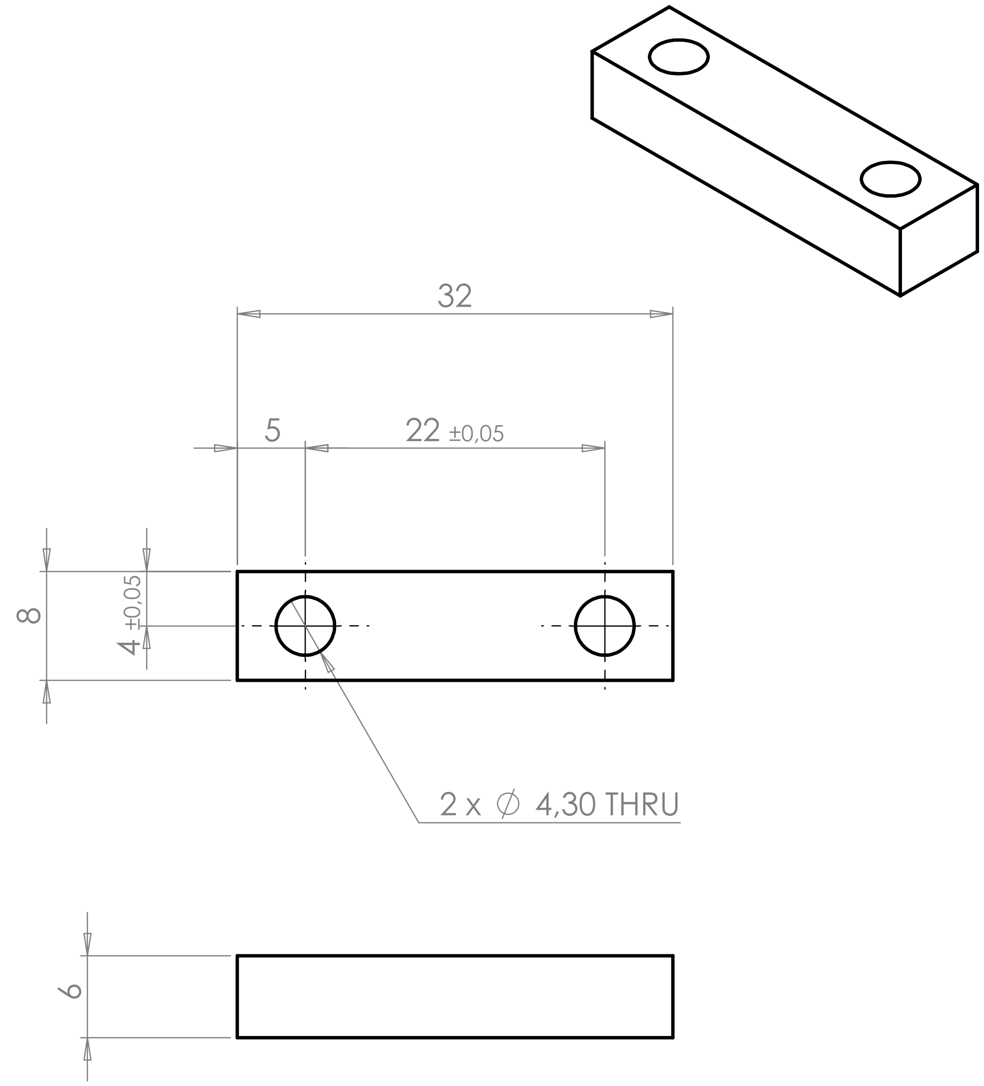

ROUGHNESS: 3.2	MATERIAL: Aluminium 7075	FINISH:	MASS [g]:	GEN.TOL.: ±0.1	QTY.: 6	REV.:
THIRD ANGLE PROJECTION	SCALE: 2:1	DRAWN BY: JBJvdS		Drawing No:		
	DIMENSIONS: mm	DESGN. BY:				
	DATE: 12-2-2018	PROJECT:				
TUDelft Delft Biorobotics Laboratory Mekelweg 2, 2628 CD Delft P +31 (0)15 2785614		DESCRIPTION: Connector468				A4

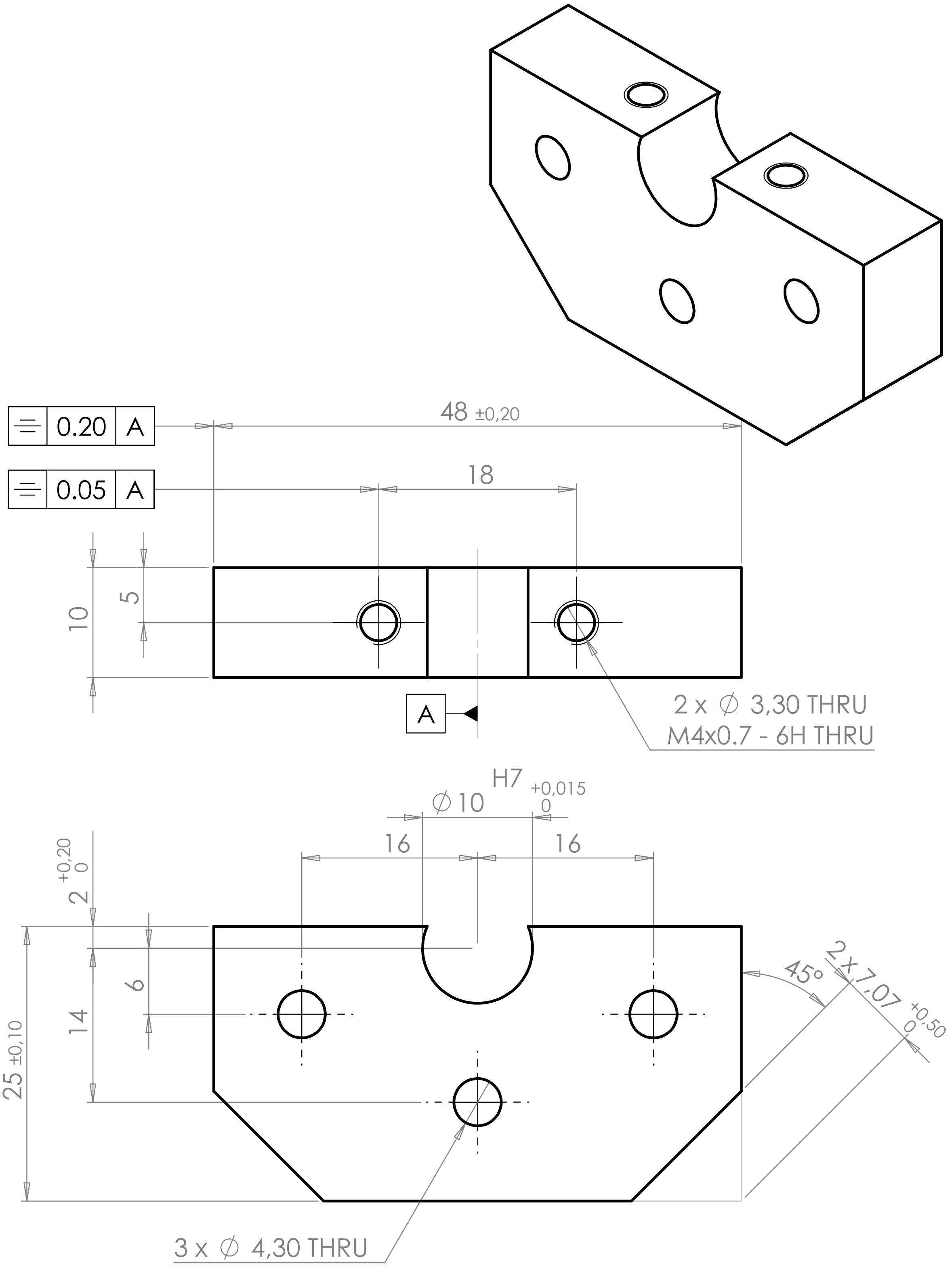
0.20 A
0.05 A
48 ±0,20
18
10
5
A
2 x ∅ 3,30 THRU
M4x0.7 - 6H THRU
∅ 10 H7 +0,015 0
16
16
2 +0,20 0
25 ±0,10
14
6
45°
2 x 7,07 +0,50 0
3 x ∅ 4,30 THRU

ROUGHNESS: 3.2	MATERIAL: Aluminium 7075	FINISH:	MASS [g]:	GEN.TOL.: ±0.05	QTY.: 2	REV.:
THIRD ANGLE PROJECTION	SCALE: 2:1	DRAWN BY: JBJvdS		Drawing No:		
	DIMENSIONS: mm	DESGN. BY:				
	DATE: 12-2-2018	PROJECT:				
TUDelft **Delft Biorobotics Laboratory** **Mekelweg 2, 2628 CD Delft** **P +31 (0)15 2785614**		DESCRIPTION: Hub2				A4

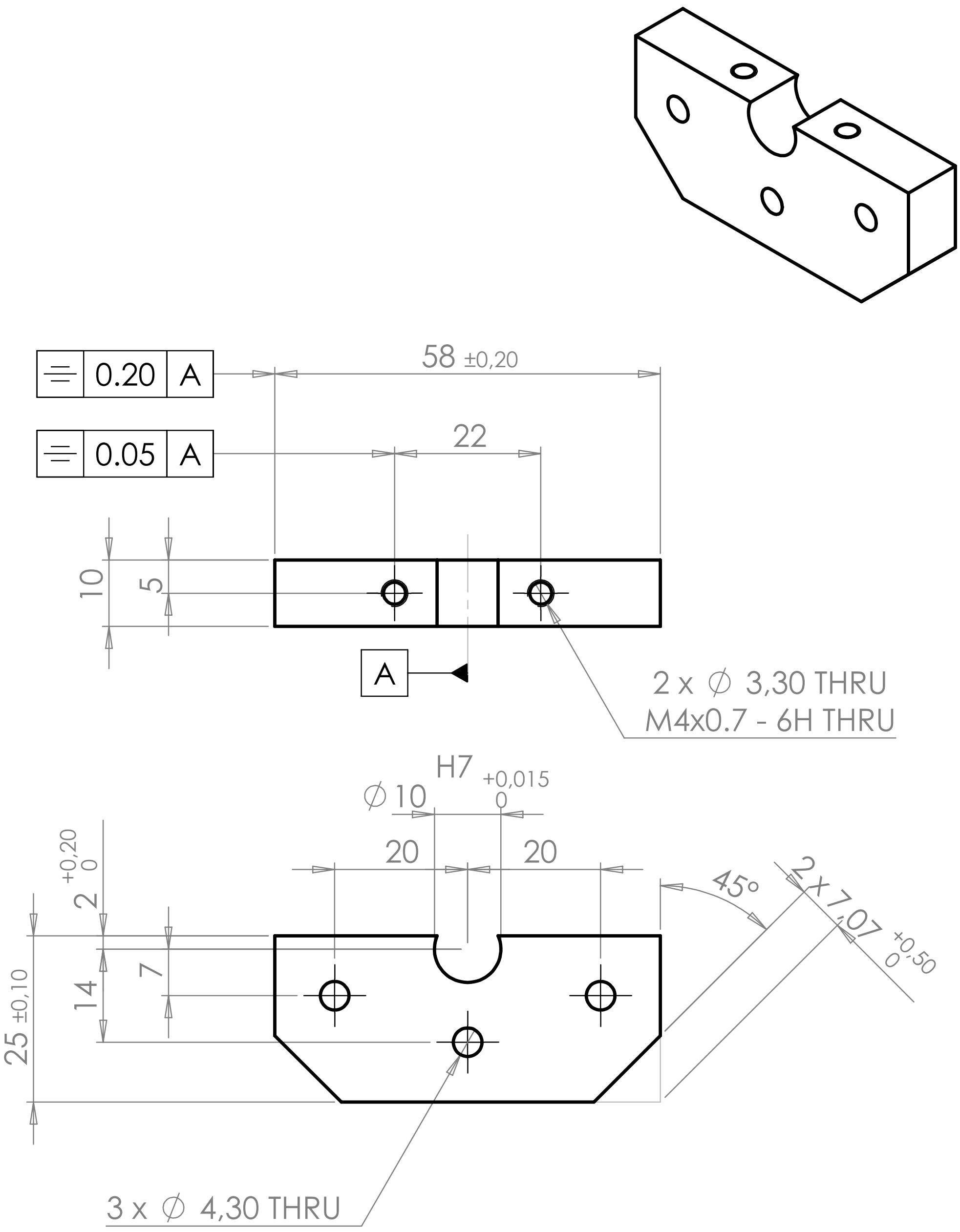
0.20 A
0.05 A
58 ±0,20
22
10
5
A
2 x ∅ 3,30 THRU
M4x0.7 - 6H THRU
∅ 10 H7 +0,015 0
20
20
45°
2 x 7,07 +0,50 0
2 +0,20 0
25 ±0,10
14
7
3 x ∅ 4,30 THRU

ROUGHNESS: 3.2	MATERIAL: Aluminium 7075	FINISH:	MASS [g]:	GEN.TOL.: ±0.05	QTY.: 6	REV.:
THIRD ANGLE PROJECTION	SCALE: 1:1	DRAWN BY: JBJvdS		Drawing No:		
	DIMENSIONS: mm	DESGN. BY:				
	DATE: 12-2-2018	PROJECT:				
Delft Biorobotics Laboratory Mekelweg 2, 2628 CD Delft P +31 (0)15 2785614	DESCRIPTION:	Hub468				A4

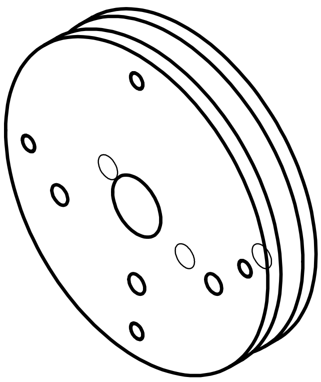

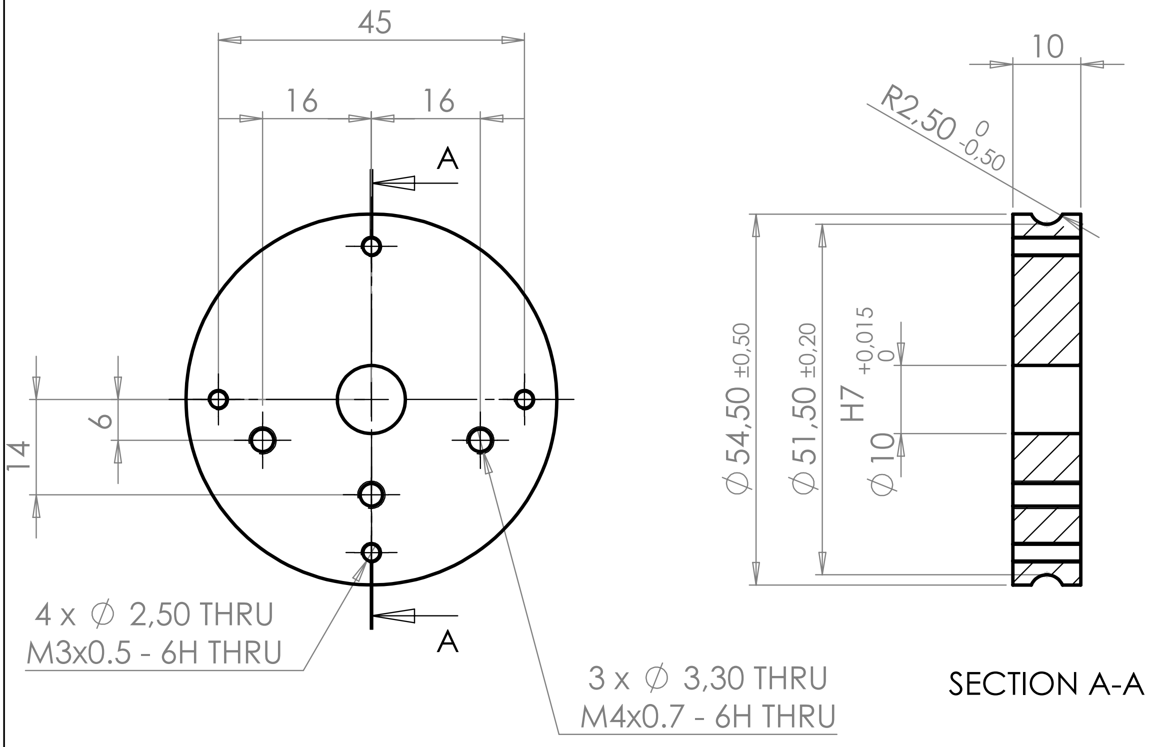
45
16
16
A
A
14
6
4 x ∅ 2,50 THRU
M3x0.5 - 6H THRU
3 x ∅ 3,30 THRU
M4x0.7 - 6H THRU
10
R2,50 0 -0,50
∅ 54,50 ±0,50
∅ 51,50 ±0,20
∅ 10 H7 +0,015 0

SECTION A-A

ROUGHNESS: 3.2	MATERIAL: Aluminium 7075	FINISH:	MASS [g]:	GEN.TOL.: ±0.05	QTY.: 2	REV.:
THIRD ANGLE PROJECTION	SCALE: 1:1	DRAWN BY: JBJvdS		Drawing No:		
	DIMENSIONS: mm	DESGN. BY:				
	DATE: 10-2-2018	PROJECT:				
Delft Biorobotics Laboratory **Mekelweg 2, 2628 CD Delft** **P +31 (0)15 2785614**		DESCRIPTION: Wheel2			A4	

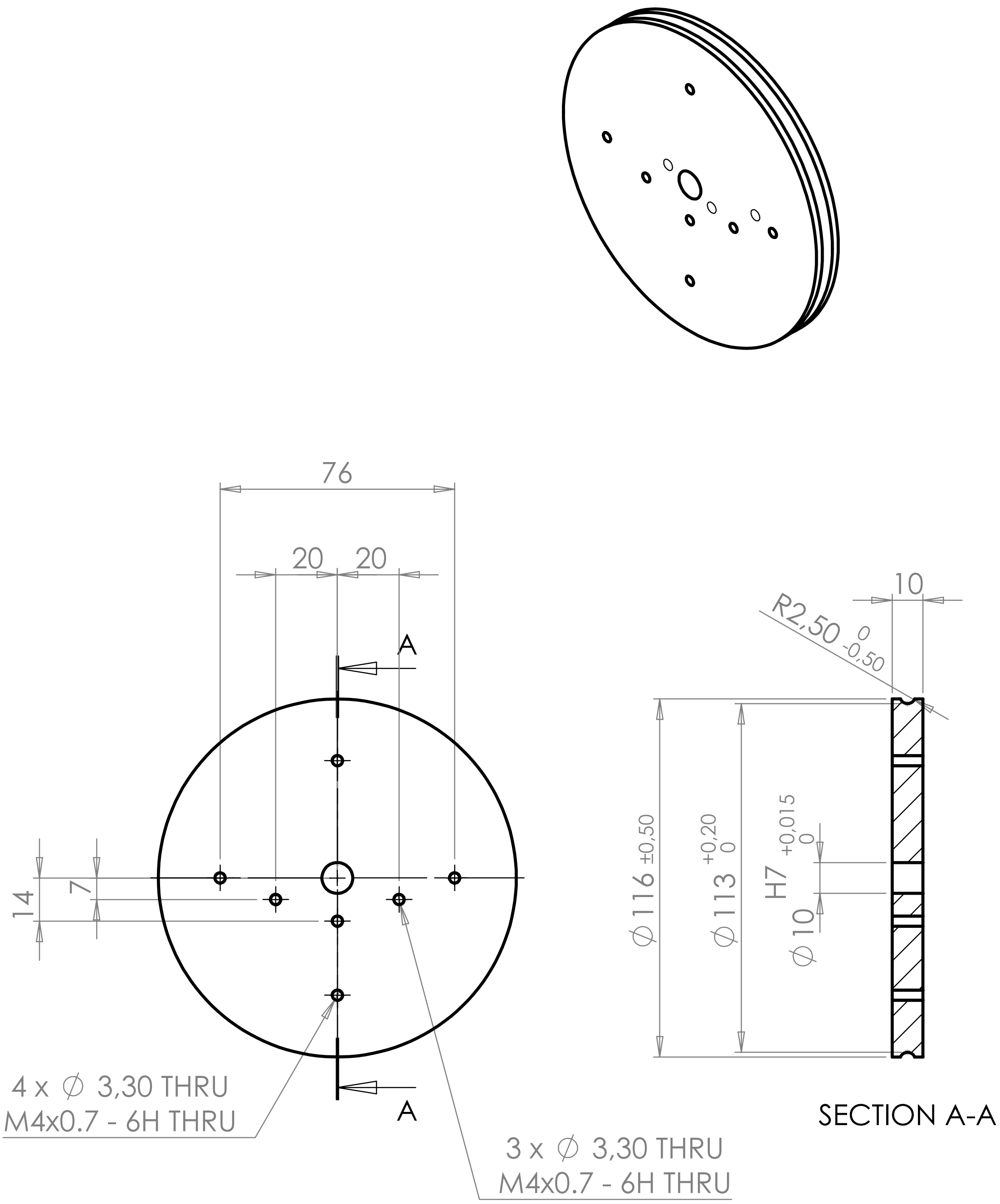
76
20
20
A
A
14
7
4 x ∅ 3,30 THRU
M4x0.7 - 6H THRU
3 x ∅ 3,30 THRU
M4x0.7 - 6H THRU
10
R2,50 0 -0,50
∅116 ±0,50
∅113 +0,20 0
∅10 H7 +0,015 0
SECTION A-A

ROUGHNESS: 3.2	MATERIAL: Aluminium 7075	FINISH:	MASS [g]:	GEN.TOL.: ±0.05	QTY.: 2	REV.:
THIRD ANGLE PROJECTION	SCALE: 1:2	DRAWN BY: JBJvdS		Drawing No:		
	DIMENSIONS: mm	DESGN. BY:				
	DATE: 12-2-2018	PROJECT:				
TUDelft **Delft Biorobotics Laboratory** **Mekelweg 2, 2628 CD Delft** **P +31 (0)15 2785614**		DESCRIPTION: Wheel4			A4	

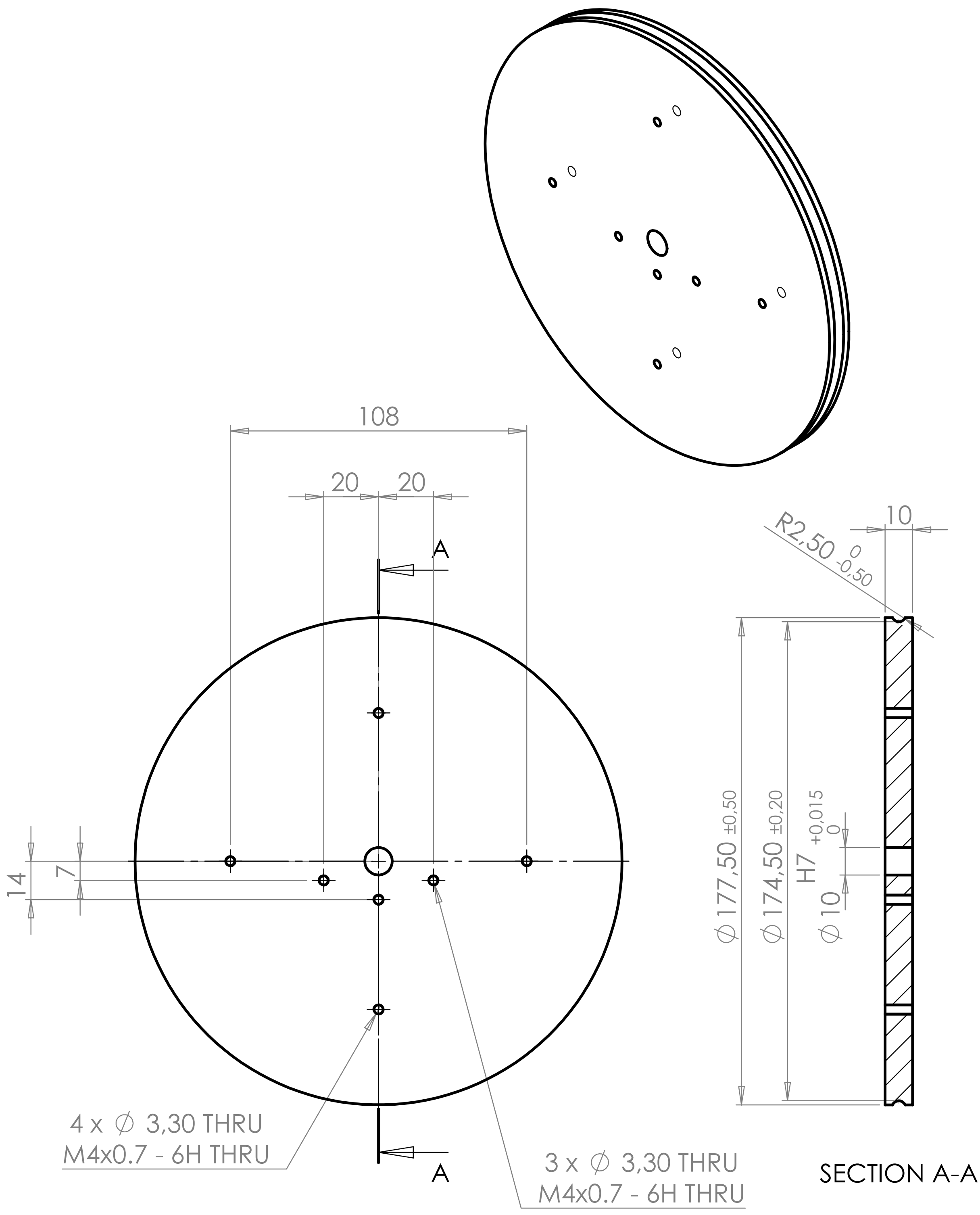
108
20
20
A
A
14
7
4 x ∅ 3,30 THRU
M4x0.7 - 6H THRU
3 x ∅ 3,30 THRU
M4x0.7 - 6H THRU
R2,50 0 -0,50
10
∅177,50 ±0,50
∅174,50 ±0,20
∅10 H7 +0,015 0
SECTION A-A

ROUGHNESS: 3.2
MATERIAL: Aluminium 7075
FINISH:
MASS [g]:
GEN.TOL.: ±0.05
QTY.: 2
REV.:
THIRD ANGLE PROJECTION
SCALE: 1:2
DIMENSIONS: mm
DATE: 12-2-2018
DRAWN BY: JBJvdS
DESGN. BY:
PROJECT:
Drawing No:

TUDelft
Delft Biorobotics Laboratory
Mekelweg 2, 2628 CD Delft
P +31 (0)15 2785614

DESCRIPTION:
Wheel6

A4

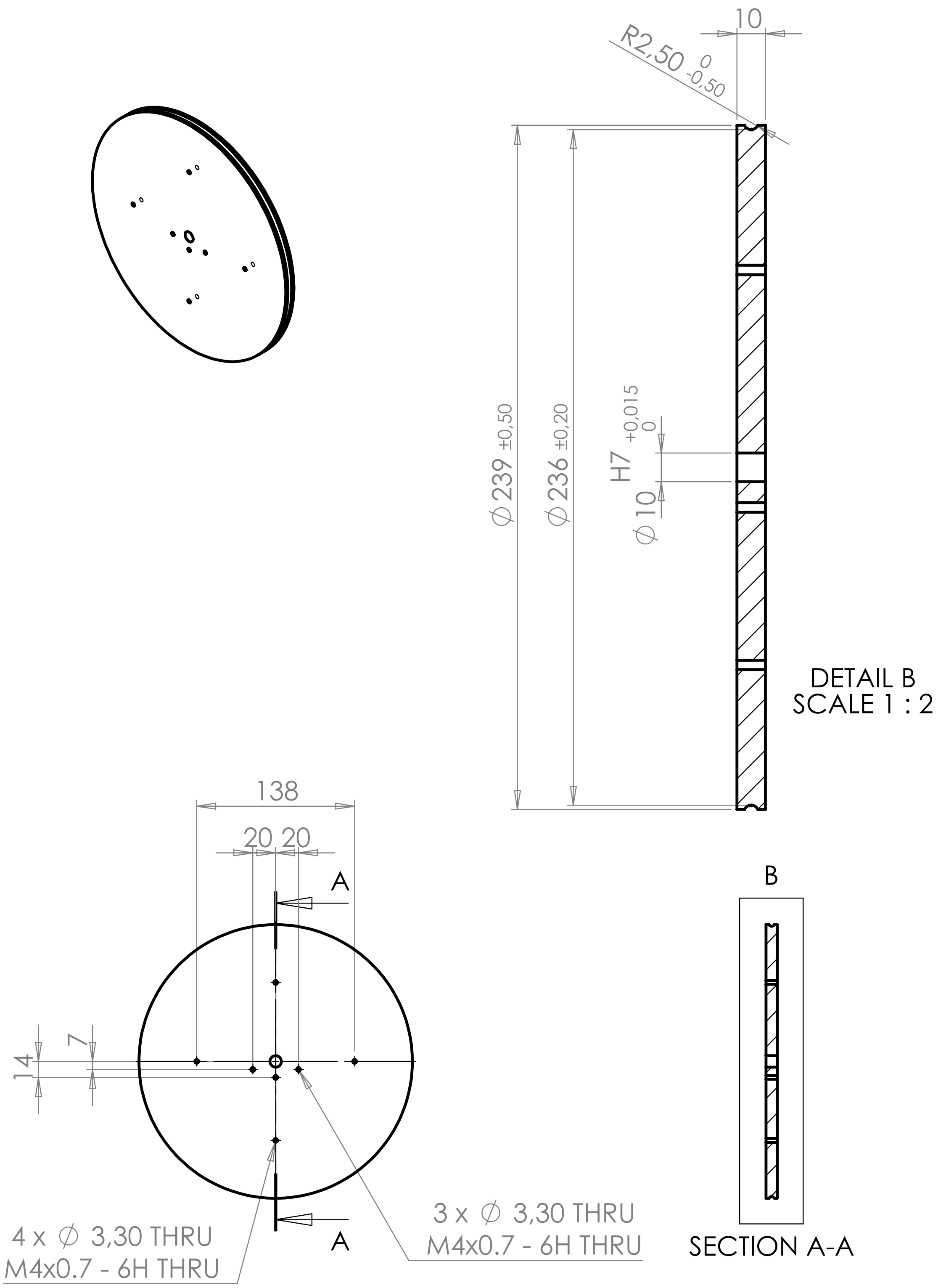
10
R2,50 0 -0,50
∅ 239 ±0,50
∅ 236 ±0,20
∅ 10 H7 +0,015 0
DETAIL B
SCALE 1 : 2
138
20 20
A
14
7
4 x ∅ 3,30 THRU
M4x0.7 - 6H THRU
A
3 x ∅ 3,30 THRU
M4x0.7 - 6H THRU
B
SECTION A-A

ROUGHNESS: 3.2	MATERIAL: Aluminium 7075	FINISH:	MASS [g]:	GEN.TOL.: ±0.05	QTY.: 2	REV.:
THIRD ANGLE PROJECTION	SCALE: 1:5	DRAWN BY: JBJvdS		Drawing No:		
	DIMENSIONS: mm	DESGN. BY:				
	DATE: 12-2-2018	PROJECT:				
TUDelft **Delft Biorobotics Laboratory** **Mekelweg 2, 2628 CD Delft** **P +31 (0)15 2785614**		DESCRIPTION:	Wheel8			A4

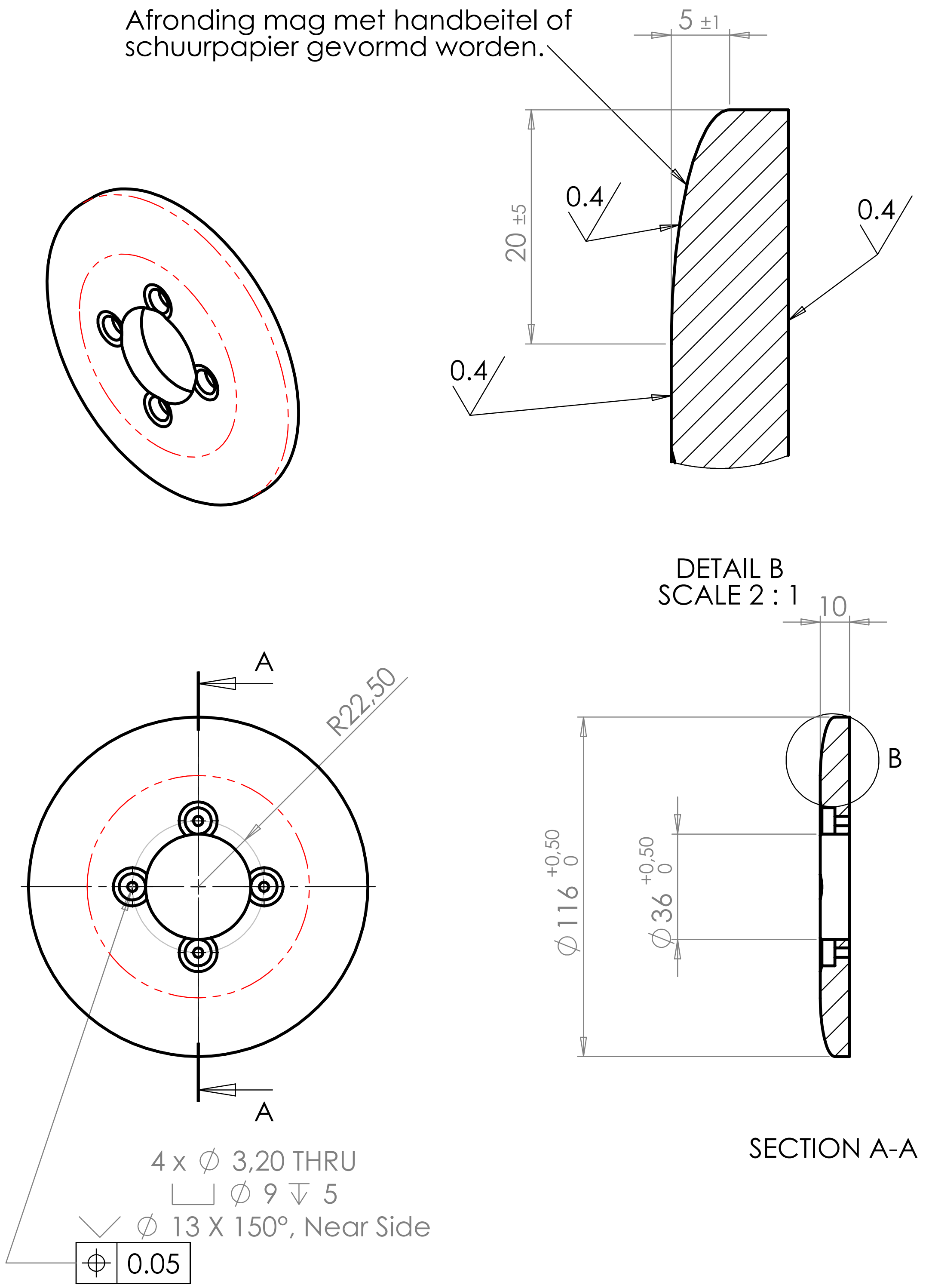

Afronding mag met handbeitel of schuurpapier gevormd worden.

5 ±1
20 ±5
0.4
0.4
0.4
0.4
DETAIL B
SCALE 2 : 1
10
A
A
R22,50
B
⌀116 +0,50 0
⌀36 +0,50 0
SECTION A-A
4 x ⌀ 3,20 THRU
⌴ ⌀ 9 ↧ 5
⌵ ⌀ 13 X 150°, Near Side
⌖ 0.05

ROUGHNESS: 3.2	MATERIAL: Epramid 6X	FINISH:	MASS [g]:	GEN.TOL.: ±0.1	QTY.: 4	REV.:
THIRD ANGLE PROJECTION	SCALE: 1:2 DIMENSIONS: mm DATE: 12-2-2018	DRAWN BY: JBJvdS DESGN. BY: PROJECT:		Drawing No:		
TUDelft	Delft Biorobotics Laboratory Mekelweg 2, 2628 CD Delft	DESCRIPTION: Flange2				A4

Afronding mag met handbeitel of schuurpapier gevormd worden.

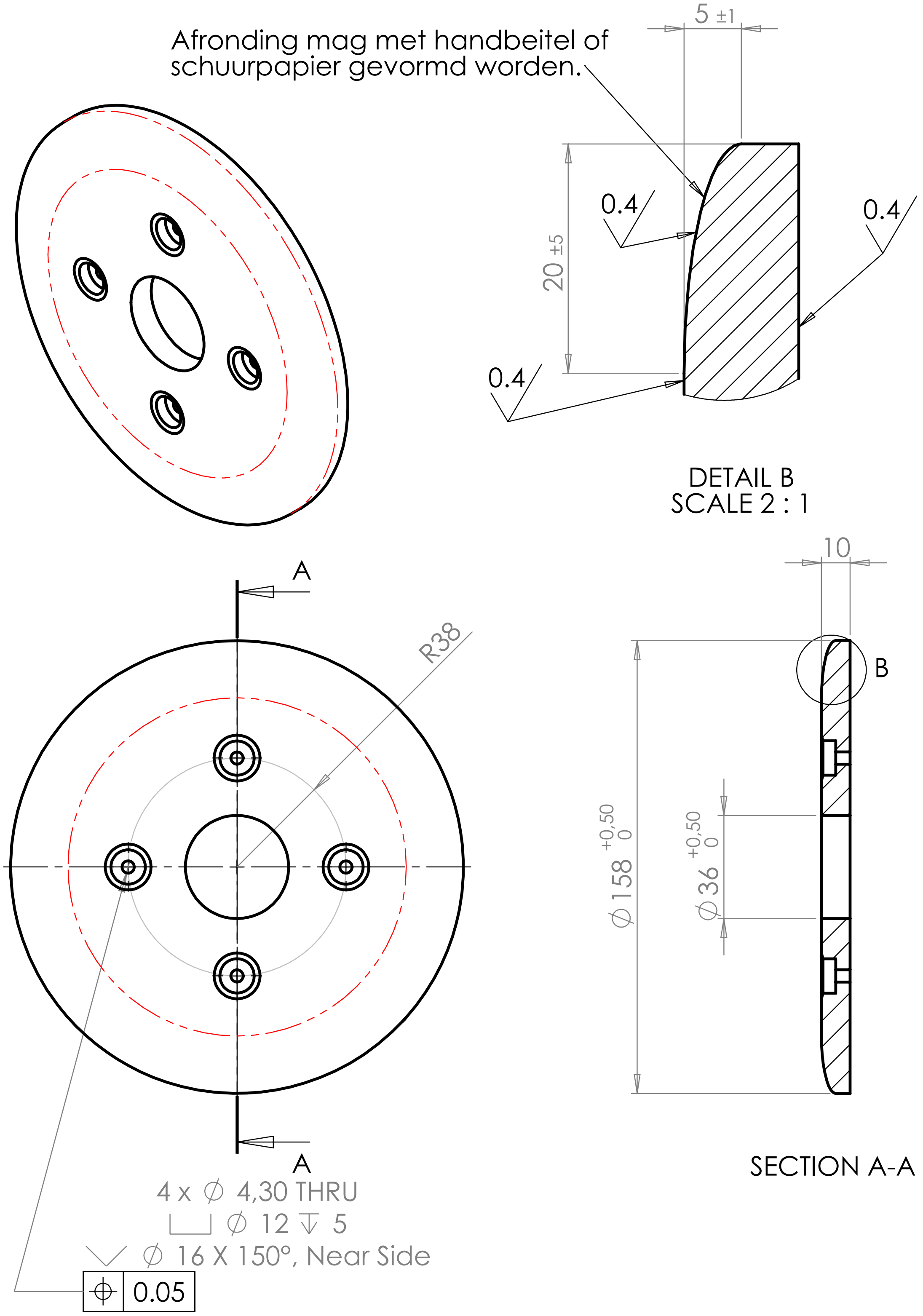
5 ±1
20 ±5
0.4
0.4
0.4
DETAIL B
SCALE 2 : 1
10
A
R38
B
⌀ 158 +0,50 0
⌀ 36 +0,50 0
A
SECTION A-A
⌖ 0.05

4 x ⌀ 4,30 THRU
⌴ ⌀ 12 ↧ 5
⌵ ⌀ 16 X 150°, Near Side

ROUGHNESS: 3.2	MATERIAL: Epramid 6X	FINISH:	MASS [g]:	GEN.TOL.: ±0.1	QTY.: 4	REV.:
THIRD ANGLE PROJECTION	SCALE: 1:2	DRAWN BY: JBJvdS		Drawing No:		
	DIMENSIONS: mm	DESGN. BY:				
	DATE: 12-2-2018	PROJECT:				
TUDelft **Delft Biorobotics Laboratory** **Mekelweg 2, 2628 CD Delft**		DESCRIPTION: Flange4				A4

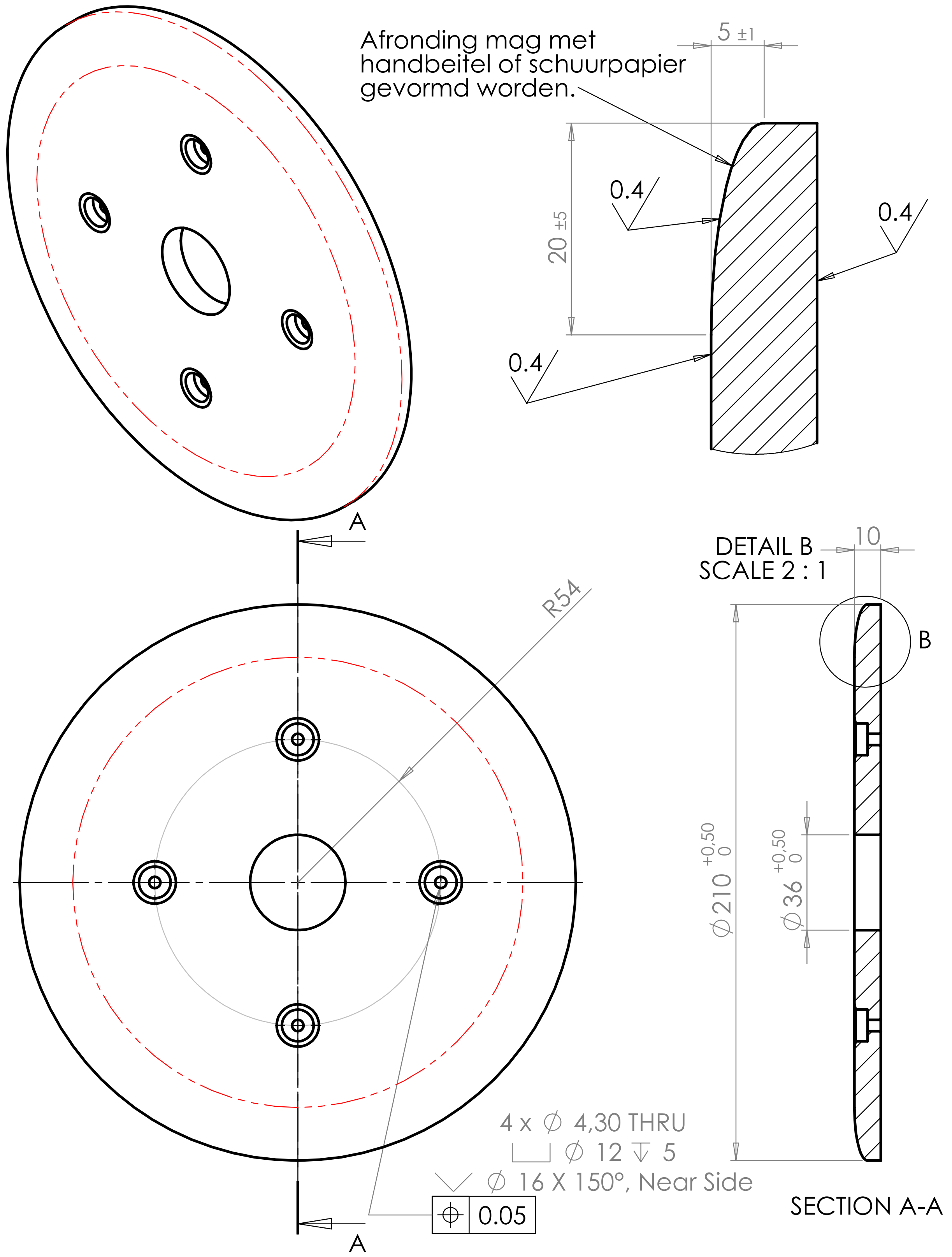
Afronding mag met handbeitel of schuurpapier gevormd worden.

5 ±1
20 ±5
0.4
0.4
0.4
0.4
A
DETAIL B
SCALE 2 : 1
10
R54
B
⌀ 210 +0,50 0
⌀ 36 +0,50 0
4 x ⌀ 4,30 THRU
⌴ ⌀ 12 ↧ 5
⌵ ⌀ 16 X 150°, Near Side
⌖ 0.05
A
SECTION A-A

ROUGHNESS: 3.2
MATERIAL: Epramid 6X
FINISH:
MASS [g]:
GEN.TOL.: ±0.1
QTY.: 4
REV.:

THIRD ANGLE PROJECTION
SCALE: 1:2
DIMENSIONS: mm
DATE: 13-2-2018
DRAWN BY: JBJvdS
DESGN. BY:
PROJECT:
Drawing No:

TUDelft
Delft Biorobotics Laboratory
Mekelweg 2, 2628 CD Delft

DESCRIPTION: Flange6

A4

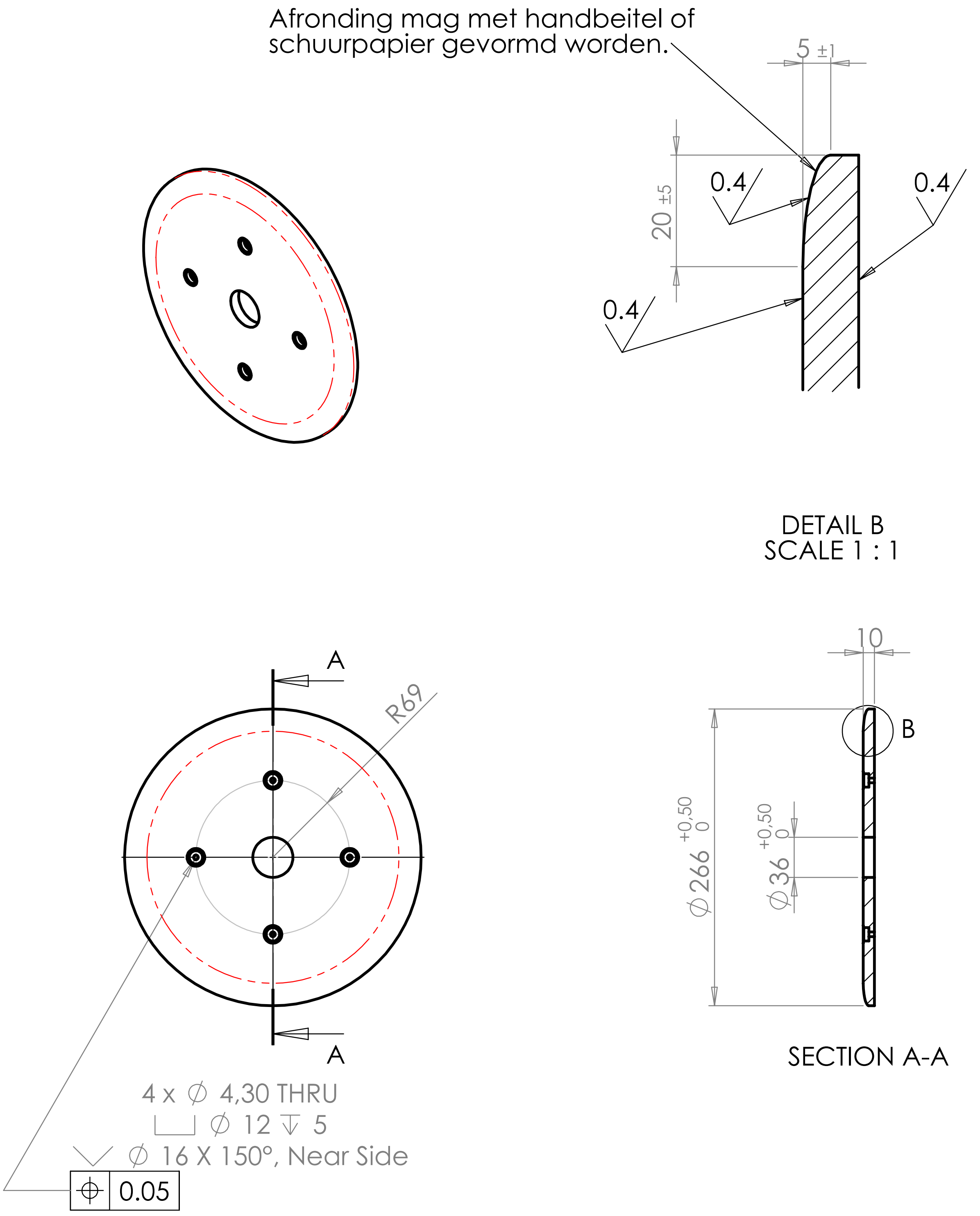

Afronding mag met handbeitel of schuurpapier gevormd worden.

5 ±1
20 ±5
0.4
0.4
0.4
0.4
DETAIL B
SCALE 1 : 1
A
A
R69
10
B
∅ 266 +0,50 0
∅ 36 +0,50 0
SECTION A-A
4 x ∅ 4,30 THRU
⌴ ∅ 12 ↧ 5
⌵ ∅ 16 X 150°, Near Side
⌖ 0.05

ROUGHNESS: 3.2
MATERIAL: Epramid 6X
FINISH:
MASS [g]:
GEN.TOL.: ±0.1
QTY.: 4
REV.:
THIRD ANGLE PROJECTION
SCALE: 1:5
DIMENSIONS: mm
DATE: 13-2-2018
DRAWN BY: JBJvdS
DESGN. BY:
PROJECT:
Drawing No:

TUDelft
Delft Biorobotics Laboratory
Mekelweg 2, 2628 CD Delft

DESCRIPTION: Flange8
A4

Bibliography

[1] Lois Finch, Hugues Barbeau, and Bertrand Arsenault. Influence of Body Weight Support on Normal Human Gait: Development of a Gait Retraining Strategy. *Physical Therapy*, 71(11):842–855, 1991.

[2] Susan Harkema, Andrea Behrman, and Hugues Barbeau. Evidence-based therapy for recovery of function after spinal cord injury. *Handbook of Clinical Neurology*, 109:259–274, 2012.

[3] Martha Visintin, Hugues Barbeau, N Korner-Bitensky, and Nancy E Mayo. A new approach to retrain gait in stroke patients through body weight support and treadmill stimulation. *Stroke; a journal of cerebral circulation*, 29(6):1122–8, 1998.

[4] Andrea L Behrman and Susan J Harkema. Spinal Cord Injury: A Series of Case Studies. *Physical Therapy*, 80(7):688–700, 2000.

[5] L. Awai, M. Franz, C. S. Easthope, H. Vallery, A. Curt, and M. Bolliger. Preserved gait kinematics during controlled body unloading. *Journal of NeuroEngineering and Rehabilitation*, 14(1):25, 2017.

[6] T George Hornby, Donielle D Campbell, Jennifer H Kahn, Tobey Demott, Jennifer L Moore, and Heidi R Roth. Enhanced gait-related improvements after therapist- versus robotic-assisted locomotor training in subjects with chronic stroke: A randomized controlled study. *Stroke*, 39(6):1786–1792, 2008.

[7] Ray D. de Leon and Christine J. Dy. What Did We Learn from the Animal Studies of Body Weight–Supported Treadmill Training and Where Do We Go from Here? *Journal of Neurotrauma*, 34(9):1744–1750, 2017.

[8] Ana M F Barela, Paulo B. De Freitas, Melissa L. Celestino, Marcela R. Camargo, and J Barela. Ground reaction forces during level ground walking with body weight unloading. *Brazilian Journal of Physical Therapy*, 18(6):572–579, 2014.

[9] Gavin Williams, Michelle Kahn, and Alana Randall. Strength Training for Walking in Neurologic Rehabilitation Is Not Task Specific. *American Journal of Physical Medicine & Rehabilitation*, 93(6):511–522, 2014.

[10] Arielle G. Fischer and Alon Wolf. Assessment of the effects of body weight unloading on overground gait biomechanical parameters. *Clinical Biomechanics*, 30(5):454–461, 2015.

[11] Michael H Dickinson, T Farley Robert, M A R Koehl, Rodger Kram, and Steven Lehman. How Animals Move: An lntegrative View. 288(April):100–106, 2000.

[12] J. Maxwell Donelan, Rodger Kram, and Arthur D. Kuo. Simultaneous positive and negative external mechanical work in human walking. *J Biomech*, 35:117–124, 2002.

[13] L. F. Requião, S. Nadeau, M. H. Milot, D. Gravel, D. Bourbonnais, and D. Gagnon. Quantification of level of effort at the plantarflexors and hip extensors and flexor muscles in healthy subjects walking at different cadences. *Journal of Electromyography and Kinesiology*, 15(4):393–405, 2005.

[14] S J Olney, M P Griffin, T N Monga, and I D McBride. Work and power in gait of stroke patients. *Archives of physical medicine and rehabilitation*, 72(5):309–314, 1991.

[15] Kyung-Ryoul Mun, Brandon Bao Sheng Yeo, Zhao Guo, Soon Cheol Chung, and Haoyong Yu. Resistance training using a novel robotic walker for over-ground gait rehabilitation: a preliminary study on healthy subjects. *Medical & Biological Engineering & Computing*, 55(10):1873–1881, 2017.

[16] Andrew A Biewener. Biomechanics of mammalian terrestrial locomotion. *Science (New York, N.Y.)*, 250(4984):1097–1103, 1990.

[17] Jamie K Burgess, Gwendolyn C Weibel, and David A Brown. Overground walking speed changes when subjected to body weight support conditions for nonimpaired and post stroke individuals. *Journal of neuroengineering and rehabilitation*, 7:6, 2010.

[18] Catarina O Sousa, José A Barela, Christiane L Prado-medeiros, Tania F Salvini, and Ana M F Barela. The use of body weight support on ground level : an alternative strategy for gait training of individuals with stroke. *Journal of NeuroEngineering and Rehabilitation*, 6(1), 2009.

[19] G.A. Cavagna, H. Thys, and Zamboni. The sources of external work in level walking and running. *The Journal of physiology*, 262(3):639–657, 1976.

[20] Jean-baptiste Mignardot, Camille G. Le Goff, Rubia van den Brand, Marco Capogrosso, Nicolas Fumeaux, Heike Vallery, Selin Anil, Jessica Lanini, Isabelle Fodor, Grégoire Eberle, Auke Ijspeert, Brigitte Schurch, Armin Curt, Stefano Carda, Jocelyne Bloch, Joachim von Zitzewitz, and Grégoire Courtine. A multidirectional gravity-assist algorithm that enhances locomotor control in patients with stroke or spinal cord injury. *Science Translational Medicine*, 9(399):eaah3621, 2017.

[21] Jinger S. Gottschall and Rodger Kram. Energy cost and muscular activity required for propulsion during walking. *Journal of Applied Physiology*, 94(5):1766–1772, 2003.

[22] Salil Apte, Michiel Plooij, and Heike Vallery. Influence of body weight unloading on human gait characteristics: a systematic review. *Journal of neuroengineering and rehabilitation*, 15(1):53, 2018.

[23] Andries Oort, Andrew Berry, Patricia Margaret Baines, Daniel Santiago Lemus Perez, and Heike Vallery. Gantry system for human gait training. 2017.

[24] Hartmut Geyer, Andre Seyfarth, and Reinhard Blickhan. Compliant leg behaviour explains basic dynamics of walking and running. *Proceedings of the Royal Society B: Biological Sciences*, 273(1603):2861–2867, 2006.

[25] Salil Apte, Michiel Plooij, and Heike Vallery. Simulation of human gait with body weight support: Benchmarking models and unloading strategies. *Journal of NeuroEngineering and Rehabilitation*, 2018.

[26] The MathWorks. No Title.

[27] H. M. Maus, S. W. Lipfert, M. Gross, J. Rummel, and A. Seyfarth. Upright human gait did not provide a major mechanical challenge for our ancestors. *Nature Communications*, 1(6):1–6, 2010.

[28] Parker Seals. Parker o-ring handbook (ORD 5700). *Parker Seal Group, Lexington, KY*, 1992.

[29] Dieter Muhs, Herbert Wittel, Manfred Becker, Dieter Jannasch, and Joachim Voßiek. *Roloff/Matek machine-onderdelen: normering, berekening, vormgeving*. Academic Service, 1996.

[30] Joachim Baumgarte. Stabilization of constraints and integrals of motion in dynamical systems. *Computer methods in applied mechanics and engineering*, 1(1):1–16, 1972.